PCCP

PAPER

View Article Online
View Journal | View Issue

Check for updates

Cite this: *Phys. Chem. Chem. Phys.*, 2025, **27**, 11428

Modeling dissipative magnetization exchange dynamics in magnetic resonance†

Neelam Sehrawat, [a] Manoj Kumar Pandey *[b] and Ramesh Ramachandran *[c]

Quantifying the role of the environment in a quantum system of interest has remained an active pursuit for studying the effects of dissipation in a wide-range of problems in chemical physics and spectroscopy. From an operational perspective, the complexities encountered in the description of open systems have ushered in the development of models without explicit consideration of the complete system. To this end, phenomenological descriptions that involve the inclusion of exponential damping terms have remained the method of choice. While such methods have gained prominence in providing a qualitative explanation for observations in spectroscopy, they are of limited utility in quantitative studies that involve the estimation of molecular constraints. As an alternative, the present report explores the possibility of understanding the nuances of dissipation found in open systems through analytic methods. Specifically, the magnetization exchange between a pair of spins (say I_1 and I_2) is examined under periodic modulation in the presence of a surrounding bath of other spins. Employing the concept of effective Hamiltonians and utilizing the block-diagonal structure of the derived effective Hamiltonians, analytic expressions are derived for describing the effects of dissipation (due to neighboring spins) on the system of interest without increasing the dimension of the problem.

Received 1st March 2025,
Accepted 24th April 2025

DOI: 10.1039/d5cp00806a

rsc.li/pccp

Open Access Article. Published on 20 May 2025. Downloaded on 5/7/2026 11:37:47 PM.
This article is licensed under a Creative Commons Attribution-NonCommercial 3.0 Unported Licence.

I. Introduction

The versatility of solid-state nuclear magnetic resonance (ssNMR) spectroscopy as a reliable tool for structure determination (at the atomic level) relies on its ability to measure and quantify the anisotropic spin interactions present in the solid state. While rapid molecular motion in the liquid state provides (only) an average estimate of the molecular constraints (such as intra/inter-atomic distances, chemical shifts, *etc.*), the restricted mobility in the solid state should, at least in principle, facilitate the determination of conformations through measurement of orientation-dependent anisotropic spin interactions (such as dipolar-coupling interactions, chemical shift anisotropy (CSA), *etc.*). A detailed account on the progress made in the field of structure determination using solid-state NMR is well-summarized in recent reports in the literature.[1–8] From a practical viewpoint, the restricted mobility in the solid state only broadens the spectrum, often suppressing the information content present in the anisotropic interactions. Although experiments that involve physical rotation of a sample (*e.g.*, magic angle spinning (MAS)[9,10]) have drastically improved the resolution of the NMR spectrum in solids,[1,2,5,11,12] the improvements in resolution have always been achieved at the expense of structural information present in the anisotropic interactions. To this end, sophisticated experiments that compensate for the averaging effects of MAS (both in the presence and absence of oscillating magnetic fields) have emerged in the past.[1,2] It is important to realize that in MAS experiments that involve structure determination, the anisotropic spin interactions (such as dipolar interactions and CSA interactions) are only partially introduced without compromising the spectral resolution. Here in this report, we focus on experiments that involve reintroduction of dipolar interactions in MAS experiments (commonly referred to as dipolar recoupling experiments). From an experimental perspective, the introduction of the dipolar interactions in MAS experiments is highly dependent on the information desired from such studies. For example, to establish the local connectivity in spectral assignment studies, the dipolar interactions are introduced in a non-selective manner, while in the measurement of intra/inter-atomic distance constraints, the dipolar

[a] *Indian Institute of Technology (IIT) Ropar, Rupnagar, Punjab, 140001, India*
[b] *Indian Institute of Technology (IIT) Ropar, Rupnagar, Punjab, 140001, India. E-mail: mkpandey@iitrpr.ac.in*
[c] *Department of Chemical Sciences, Indian Institute of Science Education and Research (IISER) Mohali, Sector 81, Manauli, P.O. Box-140306, Mohali, Punjab, India. E-mail: rramesh@iisermohali.ac.in*

† Electronic supplementary information (ESI) available: (i) Definition of anisotropic coefficients in MAS experiments, (ii) derivation of corrections based on Magnus formula, (iii) description of the CSA interaction frame using Bessel functions, (iv) description of the CSA interaction frame in the extended Hilbert space, and (v) description of R^2 in the I_1–I_2–S_N system. A detailed description of the G-coefficients along with the operators involved in the Floquet Hamiltonian H_F derived for the multi-spin (I_1–I_2–S_N) model system and NMR parameters employed in the multi-spin simulations are listed in Tables S1 and S2, respectively, of the ESI. See DOI: https://doi.org/10.1039/d5cp00806a

This journal is © the Owner Societies 2025

Open Access Article. Published on 20 May 2025. Downloaded on 5/7/2026 11:37:47 PM.
This article is licensed under a Creative Commons Attribution-NonCommercial 3.0 Unported Licence.

interactions are introduced in a selective fashion to minimize multi-spin effects. To this end, suites of dipolar recoupling experiments have emerged in the field and are well-documented in the literature.[1,13–18] Here in this report, we focus on the Rotational Resonance (R^2) experiment, a selective dipolar recoupling experiment employed for measuring homonuclear intra-atomic distances (such as ^{13}C–^{13}C).

From a historical perspective, the phenomenon of rotational resonance (R^2) was first observed in 1963 by Andrew and coworkers.[19,20] In the R^2 experiment, the dipolar interactions between a pair of spins is reintroduced when the sample rotation frequency (say, ω_r) is adjusted to the chemical shift separations between the two spins (say, $|\omega_1^{(0)} - \omega_2^{(0)}| = N\omega_r$, $N = 1$ or 2, where $\omega_1^{(0)}$ and $\omega_2^{(0)}$ denote the chemical shift of the spins 1 and 2, respectively). Consequently, the spectral resolution afforded by sample rotation is compromised (under such special conditions), leading to a broadened spectrum. Due to the presence of intermolecular dipolar interactions, the line-broadening observed under R^2 conditions remained qualitative and less informative. To this end, Griffin and coworkers[21–23] employed selectively labeled samples to monitor the magnetization exchange (minimize intermolecular effects) between a pair of spins. From a theoretical viewpoint, the initial description of the spin dynamics between the two spins under R^2 conditions was explained through a pseudo-two-spin model comprising virtual spin states.[24] In an alternate approach, employing a phenomenological damping/dissipation term[25–28] (to account for multi-spin effects) and the internuclear distance as free-fit parameters, the magnetization exchange between a pair of spins was employed to estimate the distance between them in R^2 experiments for selectively labeled samples.

While such models have been successful in providing a decent estimate of ^{13}C–^{13}C distances in the strong-coupling limit (short-range distances, 2.5–3.5 Å), the spin dynamics in the intermediate and weak-coupling limit (3.5–7.0 Å) were fraught with difficulty. To address this issue, models that employ multiple dissipative terms[29] were also proposed for fitting the magnetization exchange trajectories observed in R^2 experiments. As an alternative, to minimize the effects of other spin interactions, modifications in the form of constant-time R^2 (commonly referred to as rotational resonance width (RRW)[30]) experiments have also been proposed to separate the dipolar contributions from the dissipation (or depolarization) observed in the weak-coupling limit. Subsequently, employing this modified approach, in combination with two-dimensional NMR spectroscopy[31] and two-spin models (in the presence of phenomenological damping), the RRW experiment was employed to measure multiple distances in uniformly labeled solids.[32–35] Nevertheless, estimation of the distances in the intermediate- and weak-coupling limits has always been fraught with difficulty.

To address this issue, alternate models based on the spherical tensor operator formalism employing three different damping terms[36] were also explored to fit the exchange trajectories observed in RRW experiments. Nevertheless, significant deviations still persisted in the weak-coupling limit. From an operational perspective, the dissipative terms employed to fit trajectories differ depending on the model[37,38] and could yield ambiguous results when the magnitude of the estimated dipolar coupling is on par with the magnitude of other spin interactions (such as chemical shift anisotropy and residual heteronuclear dipolar-coupling interactions) present in the system. In such cases, the dissipative effects introduced by the phenomenological damping terms often result in ambiguous distance measurements. This theoretical prediction was well-substantiated by an in-depth analysis of R^2 experiments based on numerical methods.[39] The dissipative effects observed were attributed to the residual dipolar-coupling interactions (between ^{13}C–^{1}H) and described numerically using model systems comprising four to five protons. Since extraction of molecular constraints involves iterative fitting of experimental data, such methods are of limited utility.

To this end, an analytic framework based on the concept of effective Hamiltonians is proposed to describe the multi-spin effects observed in R^2 experiments. To present a tangible description of the spin dynamics, the depolarization effects emerging from the CSA interactions of the observed spin (say spins I_1 and I_2) as well as the surrounding S-spins (say, 'N' S-spins) is described employing effective Floquet Hamiltonians.[40–44] In contrast to methods based on effective Hamiltonians defined in the rotating frame, the proposed theoretical approach presents a framework for separating the CSA contributions emerging from the observed (say, I spins) as well as the unobserved spins (say, S-spins). Accordingly, employing the block-diagonal form of the derived effective Hamiltonians, the polarization transfer from spin I_1 to spin I_2 in the presence of the surrounding 'N' S-spins is described using simple trigonometric expressions analogous to the one obtained in the description of an isolated two-spin system (I_1–I_2). In contrast to phenomenological models (that employ a single damping term), the damping effects due to the observed (I-spins) and the unobserved spins (say, the S-spins that are decoupled) are well-separated and rigorously verified through simulations emerging from exact numerical methods.

To improve the readability, the article is structured as follows. In Section-II, the basic theory underlying the derivation of effective Hamiltonians in the rotating frame and CSA interaction frame is discussed. Through comparison with simulations emerging from analytic expressions and numerical methods, the exactness of the effective Hamiltonians is verified. This is then followed by the extension of the theoretical method for estimating distances in real systems. Employing simple analytic expressions, the dissipative effects in multi-spin systems emerging from residual dipolar-coupling interactions (say, ^{13}C–^{1}H dipolar-coupling interactions) are identified and discussed through rigorous comparisons with simulations emerging from exact numerical methods. In contrast to other existing phenomenological models, the proposed analytic model presents an attractive framework for estimating both the ^{13}C–^{13}C and ^{13}C–^{1}H distances besides the signs/magnitude of the CSA tensors of the spins. This is then followed by a brief summary in the final section.

Open Access Article. Published on 20 May 2025. Downloaded on 5/7/2026 11:37:47 PM. This article is licensed under a Creative Commons Attribution-NonCommercial 3.0 Unported Licence.

II. Theory and simulations

One of the primary motivations for quantifying the spin dynamics in R^2 experiments lies in its ability to provide internuclear distance information, a typical practical scenario being the measurement of ^{13}C–^{13}C distances in biological solids. Being less sensitive and less abundant, the distance measurements are often carried out in uniformly ^{13}C-labeled samples (with an appropriate dilution in natural abundance to minimize intermolecular effects). While isotopic enrichment helps in improving the sensitivity of the ^{13}C spins, the interaction with the surrounding (abundant) ^{1}H-spins often complicates the interpretation of the experimental data. Hence, decoupling of the ^{13}C–^{1}H dipolar interactions is routinely employed in experiments that involve measurement of ^{13}C–^{13}C distances. Nevertheless, the dissipation due to residual dipolar-coupling contributions (from ^{13}C–^{1}H) persists and still plays an important role. Additionally, the magnitude and sign of the CSA interactions of the ^{13}C spins also have a prominent role in the magnetization exchange observed among spins in R^2 experiments. To outline the relative contributions of the various spin interactions in the R^2 experiments, we divide the discussion into two parts. In the first part of the discussion, the role of the spin interactions associated with the system of interest (active 'I' spins such as ^{13}C) is discussed within an isolated two-spin model (*i.e.*, I_1–I_2). In the second part of the discussion, the role of the surroundings (*i.e.*, abundant 'S' spins, say protons, ^{1}H) is discussed employing a multi-spin model comprising 'N' S-spins (say, I_1–I_2–S_N).

A. Effective Hamiltonian for the isolated two-spin system

To quantify and exemplify the relevance of the chemical shift anisotropy (CSA) interactions (of the observed spins) in R^2 experiments, we begin with a model system comprising two spins (say, $I_1 = I_2 = 1/2$). Accordingly, the Hamiltonian for such a system under MAS[45,46] conditions is expressed as a sum in terms of the single-spin and two-spin interactions.

$$H(t) = H_{\mathrm{System}}(t) = \underbrace{H_{\mathrm{CS}}(t)}_{\text{single-spin}} + \underbrace{H_{\mathrm{D}}(t)}_{\text{two-spin}}. \quad (1)$$

In the present case, the single-spin interaction comprises the chemical shift interaction and has both an isotropic (represented by H_{iso}) and anisotropic (represented by H_{CSA}) component. Due to physical rotation of the sample, only the anisotropic part of the chemical shift interaction becomes time-dependent and is summarised by the following equations:

$$H_{\mathrm{CS}}(t) = \underbrace{\sum_{i=1}^{2} \omega_i^{(0)} I_{iz}}_{H_{\mathrm{iso}}} + \underbrace{\sum_{i=1}^{2} \sum_{\substack{m=-2,\\ m\neq 0}}^{2} \omega_i^{(m)} e^{im\omega_r t} I_{iz}}_{H_{\mathrm{CSA}}(t)}. \quad (2)$$

In the above equation, $\omega_i^{(0)}$ denotes the isotropic component of the chemical shift interaction (commonly referred to as chemical shift), while, $\omega_i^{(m)}$[45,47] denotes the orientation-dependent (or anisotropic) component of the chemical shift interaction (commonly referred to as chemical shift anisotropy (CSA)). The index 'm' denotes the component of the CSA interaction associated with a particular spin, i = 1 or 2. The notation I_{iz} is representative of the z-component of the spin angular momentum operator associated with the spins I_1 and I_2. The coupling between spins in the solid state is predominantly established through the dipolar-coupling interactions and is represented by the two-spin Hamiltonian given below:[45]

$$H_{\mathrm{D}}(t) = \sum_{\substack{m=-2,\\ m\neq 0}}^{2} \omega_{12}^{(m)} e^{im\omega_r t}\left(2I_{1z}I_{2z} - \frac{1}{2}\left(I_1^+ I_2^- + I_1^- I_2^+\right)\right). \quad (3)$$

Analogous to the CSA interactions, the anisotropic components of the dipolar-coupling interactions are time-dependent and are represented by $\omega_{12}^{(m)}$ coefficients. The detailed description of the anisotropic coefficients (refer to the ESI†) is well-documented[45–47] and is omitted here to minimize repetition.

As illustrated above, physical rotation of the sample renders the anisotropic interactions (CSA and dipolar-coupling interactions) time-dependent and averages them out in MAS experiments. Since structural constraints (such as intra-atomic distances, torsion angles and chemical shift tensors (both magnitude and sign along with asymmetry parameter)) are concealed in the anisotropic interactions, experiments that involve their presence (or reintroduction) without compromising spectral resolution become inevitable in the solid state. To realize this (dual) objective, the anisotropic spin interactions of interest are reintroduced in a controlled fashion in MAS experiments without compromising the spectral resolution. From an experimental perspective, this implies the compensation of the averaging effects of MAS and is often realized through the application of oscillating radio-frequency (RF) fields.[13–18] Interestingly enough, in the case of R^2 experiments, the dipolar interactions are reintroduced without RF pulses through careful choice of the spinning frequency. In a typical R^2 MAS experiment, the dipolar-coupling interaction between a pair of spins (i and j) is reintroduced when the sample spinning frequency is adjusted to the isotropic chemical shift difference between the spins (*i.e.*, $|\omega_1^{(0)} - \omega_2^{(0)}| = N\omega_r$, N = 1 or 2). Under such conditions, a part of the dipolar-coupling Hamiltonian (refer to eqn (3)) becomes time-independent and provides the source for estimating distances from R^2 experiments. Although several theoretical formulations[24–30,32–36] exist for describing the underlying spin dynamics, a compact analytic expression explicating the contributions emerging from the CSA and dipolar-coupling interactions in R^2 experiments has remained elusive. This forms the main motivation behind the present study.

To explicate the interference effects resulting from the sample spinning frequency, the quantum-Liouville equation (refer to eqn (4a)) is transformed by the unitary transformation operator, U_1 ($U_1 = e^{in\omega_r t I_{1z}} e^{-in\omega_r t I_{2z}}$).

$$i\hbar\frac{d\rho(t)}{dt} = [H(t), \rho(t)] \quad (\hbar = 1). \quad (4a)$$

 This journal is © the Owner Societies 2025

Open Access Article. Published on 20 May 2025. Downloaded on 5/7/2026 11:37:47 PM.
This article is licensed under a Creative Commons Attribution-NonCommercial 3.0 Unported Licence.

Accordingly, in the interaction frame defined by U_1, the above equation reduces to the following form.

$$i\frac{d\tilde{\rho}(t)}{dt} = \left[\underbrace{U_1 H(t) U_1^{-1}}_{\tilde{H}(t)}, \underbrace{U_1 \rho(t) U_1^{-1}}_{\tilde{\rho}(t)}\right]. \quad (4b)$$

The above choice of the transformation operator[32,36,37] is based on the sign of the offsets employed for the spins (in the present context, the spins I_1 and I_2 have +ve and −ve offsets, respectively). Depending on the desired resonance conditions (*i.e.*, $|\omega_1^{(0)} - \omega_2^{(0)}| = N\omega_r$, $N = 1$ or 2), the choice of 'n' employed in U_1 varies (for *e.g.*, when $N = 1$, $n = 0.5$; $N = 2$, $n = 1.0$). Such a transformation facilitates the description of the off-resonant behaviour observed in the resonance width experiment.

Accordingly, the Hamiltonians (eqn (2) and (3)) get transformed (in the new interaction frame) and are summarized by the equations given below:

$$\tilde{H}_{iso} = U_1 H_{iso} U_1^{-1} = (\omega_1^{(0)} - n\omega_r) I_{1z} + (\omega_2^{(0)} + n\omega_r) I_{2z}, \quad (5)$$

$$\tilde{H}_{CSA}(t) = U_1 H_{CSA}(t) U_1^{-1} = H_{CSA}(t), \quad (6)$$

and

$$\begin{aligned}\tilde{H}_D(t) &= U_1 H_D(t) U_1^{-1} \\ &= \sum_{\substack{m=-2,\\ m\neq 0}}^{2} \omega_{12}^{(m)} e^{im\omega_r t}(2I_{1z}I_{2z}) \\ &\quad + \left(-\frac{1}{2}\right) \sum_{\substack{m=-2,\\ m\neq 0}}^{2} \omega_{12}^{(m)} \left(I_1^+ I_2^- e^{i(m+2n)\omega_r t} + I_1^- I_2^+ e^{i(m-2n)\omega_r t}\right).\end{aligned} \quad (7)$$

Depending on the matching conditions (*i.e.*, $|\omega_1^{(0)} - \omega_2^{(0)}| = 2n\omega_r$, where $n = 0.5$ or 1), a part of the dipolar interaction (refer to eqn (7)) becomes time-independent and plays an important role in the magnetization exchange observed between spins in R^2 experiments. To highlight the significant role of the CSA interactions in R^2 experiments, here in this report, we focus on the matching condition, $|\omega_1^{(0)} - \omega_2^{(0)}| = 2\omega_r$. The discussion that follows is equally valid for the $N = 1$ resonance condition.

Consequently, the dipolar-coupling Hamiltonian (refer to eqn (7)) reduces to a form that comprises both time-dependent ($\tilde{H}_{D,T}(t)$) and time-independent terms ($\tilde{H}_{D,S}$), as shown below:

$$\tilde{H}_D(t) = \tilde{H}_{D,S} + \tilde{H}_{D,T}(t), \quad (8)$$

where

$$\tilde{H}_{D,S} = \left(-\frac{1}{2}\right) \cdot \left[\omega_{12}^{(-2)} (I_1^+ I_2^-) + \omega_{12}^{(2)} (I_1^- I_2^+)\right], \quad (9)$$

and

$$\begin{aligned}\tilde{H}_{D,T}(t) &= \sum_{\substack{m=-2,\\ m\neq 0}}^{2} (2I_{1z}I_{2z}) \omega_{12}^{(m)} e^{im\omega_r t} \\ &\quad + \left(-\frac{1}{2}\right) \left[\sum_{\substack{m=-2,\\ m\neq 0,-2}}^{2} \omega_{12}^{(m)} (I_1^+ I_2^-) e^{i(m+2n)\omega_r t}\right. \\ &\quad \left. + \sum_{\substack{m=-2,\\ m\neq 0,2}}^{2} \omega_{12}^{(m)} (I_1^- I_2^+) e^{i(m-2n)\omega_r t}\right].\end{aligned} \quad (10)$$

From an experimental perspective, the above matching condition facilitates the implementation of the R^2 experiments at lower spinning frequencies and also minimizes the interference effects emerging from other residual heteronuclear dipolar-coupling interactions (between the spins of interest (say, I_1, I_2) and the surrounding abundant spins, S). Since the number of structural constraints (such as intramolecular distances) available in the solid state is limited due to resolution, the accuracy of the estimated constraints plays an important role in the quality of structures derived from ssNMR measurements. To realize this objective, analytic models that provide a general description of the spin dynamics independent of the internal (magnitudes of the spin interactions (such as magnitudes of the CSAs of spins)) and external parameters (such as spinning frequency and RF fields employed) remain essential. When the chemical shift difference is smaller than the magnitude of the CSA interactions, both the $N = 1$ and 2 resonance conditions ($|\omega_1^{(0)} - \omega_2^{(0)}| = N\omega_r$) are influenced by the CSA interactions. In such cases, an additional transformation into the CSA interaction frame is required for faster convergence of the corrections to the effective Hamiltonian. Depending on the magnitude of the CSA interactions (indicated by δ_{CSA}) relative to both the spinning frequency and the measured dipolar-coupling constant, the approximations employed (in the analytic models) to quantify the magnetization transfer among spins may be divided into three categories discussed below. A pedagogical discussion is presented below by examining the exactness of analytic models through comparisons with simulations emerging from exact numerical methods.

A.1. Case-1 ($\omega_r \gg |\delta_{CSA}|$). When the spinning frequency, ω_r largely exceeds the magnitudes of the anisotropic interactions (inclusive of both the CSA and dipolar-coupling interactions), the time-dependent terms associated with the single spin (say, $H_{CSA}(t)$) and the two-spin interactions (say, dipolar-coupling interactions ($H_{D,T}(t)$)) are ignored in further calculations. In such cases, the effective Hamiltonian describing the spin dynamics is governed only by the static terms in the Hamiltonian.

$$\begin{aligned}H_{eff} &= \tilde{H}_{iso} + \tilde{H}_{D,S} \\ &= \left(\omega_1^{(0)} - n\omega_r\right) I_{1z} + \left(\omega_2^{(0)} + n\omega_r\right) I_{2z} \\ &\quad + \left(-\frac{1}{2}\right) \left[\omega_{12,e}^{(-2)} \cdot (I_1^+ I_2^-) + \omega_{12,e}^{(2)} \cdot (I_1^- I_2^+)\right],\end{aligned} \quad (11)$$

where $\omega_{12,e}^{(-2)} = \omega_{12}^{(-2)}$ and $\omega_{12,e}^{(2)} = \omega_{12}^{(2)}$.

Open Access Article. Published on 20 May 2025. Downloaded on 5/7/2026 11:37:47 PM.
This article is licensed under a Creative Commons Attribution-NonCommercial 3.0 Unported Licence.

Subsequently, the magnetization transfer from spin I_1 to spin I_2 is evaluated using the standard expression given below.

$$\langle \tilde{I}_{2z}(t) \rangle = \mathrm{Tr}[\tilde{\rho}(t) \cdot \tilde{I}_{2z}]. \tag{12}$$

where, $\tilde{\rho}(t) = U(t)\tilde{\rho}(0)U^{-1}(t)$, is the density operator at time 't' and $\rho(0)$ is the initial density operator. The term $U(t)$ represents the time propagator, *i.e.*, $U(t) = \exp(-iH_{\mathrm{eff}}t)$.

In the present context, magnetization transfer from spin 'I_1' to spin 'I_2' is calculated (*i.e.*, the initial state, $\tilde{\rho}(0) = I_{1z}$). Accordingly, the magnetization loss on spin I_1 (due to transfer to spin 'I_2') is calculated based on the equation given below:

$$\langle \tilde{I}_{1z}(t) \rangle = 1 - \frac{{\omega_d}^2}{(\Omega^2 + {\omega_d}^2)} \sin^2\left(\sqrt{(\Omega^2 + {\omega_d}^2)}\right) t. \tag{13}$$

In a similar vein, the magnetization build up on spin I_2 (that had an initial magnetization of zero) is calculated employing the equation given below:

$$\langle \tilde{I}_{2z}(t) \rangle = \frac{{\omega_d}^2}{(\Omega^2 + {\omega_d}^2)} \sin^2\left(\sqrt{(\Omega^2 + {\omega_d}^2)}\right) t. \tag{14}$$

In the above equations, the term $\Omega = \frac{1}{2}\left(\omega_1^{(0)} - \omega_2^{(0)} - 2n\omega_r\right)$ denotes the effective offset experienced by the spins, while ω_{d} denotes the effective dipolar-coupling constant between the spins $\left(i.e.,\ \omega_d = \left(-\frac{1}{2}\right)\omega_{12,e}^{(-2)} \times \left(-\frac{1}{2}\right)\omega_{12,e}^{(2)}\right)$.

While the form of the above expression (eqn (14)) resembles the one obtained by Rabi[48] for describing the detuning effect in a two-level system (TLS), it is important to note that the spin dynamics of a two-spin-1/2 system (described by a vector space of dimension $((2I_1 + 1) \times (2I_2 + 1))$) is effectively reduced to a single two-level system. The term 'ω_{d}' represents the frequency (containing the dipolar coupling constant) of oscillation, while the term 'Ω' models the detuning effect (or depolarization) observed in experiments.

A.2. Case-2 ($|\delta_{\mathrm{CSA}}| \leq \omega_r$). When the magnitude of the CSA interactions is significant and on par with the spinning frequency, the (neglected) time-dependent terms (say, $H_{\mathrm{CSA}}(t)$) become relevant. Employing the prescription outlined by the Magnus expansion scheme[49] (refer to the ESI†), an effective Hamiltonian incorporating the contributions from the time-dependent terms is derived. To second-order, the effective Hamiltonian incorporating the contributions from time-dependent terms is derived and represented by the following equation.

$$\begin{aligned} H_{\mathrm{eff}} &= \left(\omega_1^{(0)} - \omega_r\right) I_{1z} + \left(\omega_2^{(0)} + \omega_r\right) I_{2z} \\ &+ \left(-\frac{1}{2}\right)\left[\omega_{12,e}^{(-2)} \cdot \left(I_1^+ I_2^-\right) + \omega_{12,e}^{(2)} \cdot \left(I_1^- I_2^+\right)\right]. \end{aligned} \tag{15}$$

In contrast to the description in the previous subsection, the effective dipolar-coupling constant ($\omega_{12,e}$) in the present case has contributions from the time-dependent terms and is summarized by the following equation:

$$\begin{aligned} \omega_{12,e}^{(-2)} &= \omega_{12}^{(-2)}\left(1 - \sum_{\substack{k=-2,\\ k\neq 0}}^{2} \frac{\left(\omega_1^{(k)} - \omega_2^{(k)}\right)}{k\omega_r}\right) \\ &+ \frac{\left(-\omega_{12}^{(1)}\right)\left(\omega_1^{(-1)} - \omega_2^{(-1)}\right)}{\omega_r}, \end{aligned} \tag{16a}$$

and

$$\omega_{12,e}^{(2)} = \omega_{12}^{(2)}\left(1 + \sum_{\substack{k=-2,\\ k\neq 0}}^{2} \frac{\left(\omega_1^{(k)} - \omega_2^{(k)}\right)}{k\omega_r}\right) + \frac{\left(-\omega_{12}^{(-1)}\right)\left(\omega_1^{(1)} - \omega_2^{(1)}\right)}{\omega_r}. \tag{16b}$$

As the form of the effective Hamiltonian (refer to eqn (15)) is similar to eqn (11), the exchange trajectories are calculated using identical equations given above (refer to eqn (13) and (14)). To verify the exactness of the derived effective Hamiltonians (eqn (11) and (15)), simulations emerging from the above analytic expressions were compared to those obtained from exact numerical methods based on SPINEVOLUTION software.[50]

As depicted in Fig. 1, when the spinning frequency exceeds the magnitude of the CSA interactions, the analytic expressions (indicated by blue dotted lines based on the first-order effective

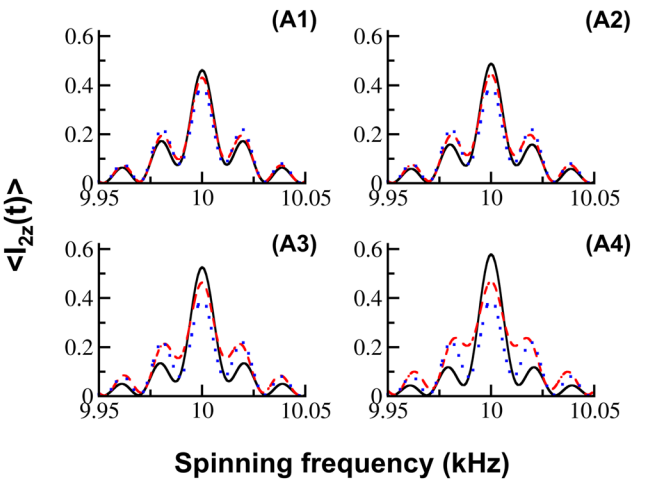

Fig. 1 In the simulations illustrated, magnetization build-up on spin 'I_2' (say, magnetization transfer from spin 'I_1' to spin 'I_2', eqn (14)) in the R^2 (corresponding to the $N = 2$ matching condition) experiment is depicted as a function of the spinning frequency. The simulations resulting from SPINEVOLUTION (indicated in black) are compared with the analytic simulations based on effective Hamiltonians comprising (i) first-order corrections only (eqn (11), indicated by blue dotted lines), and (ii) both first- and second-order corrections (eqn (15), indicated by red broken lines). The following specific parameters were employed in the panels: (A1) ($\delta_1 = 2$ kHz, $\delta_2 = 4$ kHz), (A2) ($\delta_1 = 2$ kHz, $\delta_2 = 6$ kHz), (A3) ($\delta_1 = 2$ kHz, $\delta_2 = 10$ kHz) and (A4) ($\delta_1 = 2$ kHz, $\delta_2 = 14$ kHz). The spin interaction parameters given below were held constant in the simulations: isotropic chemical shifts ($\omega_1^{(0)} = -\omega_2^{(0)} = 10$ kHz), CSA parameters ($\eta_1 = 0.0$, $\Omega^{(1)} = (0^\circ, 0^\circ, 0^\circ)$; $\eta_2 = 1.0$, $\Omega^{(2)} = (0^\circ, 90^\circ, 0^\circ)$); dipolar-coupling parameter ($r_{I_1 I_2} = 3.879$ Å), and mixing time ($t_{\mathrm{mix}} = 30$ ms). The simulations correspond to a powder sample and were implemented using 6044 orientations (zcwt6044).

This journal is © the Owner Societies 2025

Open Access Article. Published on 20 May 2025. Downloaded on 5/7/2026 11:37:47 PM.
This article is licensed under a Creative Commons Attribution-NonCommercial 3.0 Unported Licence.

Hamiltonians given in eqn (11)) give results in good agreement (refer to panel (A1)) with those obtained from exact numerical methods. However, when the magnitudes of the CSA interactions become significant and are on par with the spinning frequency, ω_r, the role of the time-dependent contributions (evaluated from the Magnus formula[49] (refer to the ESI†)) becomes significant, as evident in the simulations. Nevertheless, significant deviations are still observed in the analytic simulations (refer to panels (A3) and (A4) of Fig. 1) despite the inclusion of second-order corrections (indicated by red dashed lines). Since higher-order corrections in the Magnus formula involve the evaluation of multiple time integrals, possible extensions beyond second-order are cumbersome, thereby limiting their utility in analytic methods for describing the spin dynamics. To this end, an alternate approach is proposed in the following section.

A.3. Case-3 ($|\delta_{CSA}| > \omega_r$). To address the discrepancies observed in the analytic simulations, an alternate approach is proposed in this section. In the proposed method, the Hamiltonian in the interaction frame (eqn (4)) is transformed into an interaction frame defined by the CSA interactions (commonly referred to as a jolting frame transformation[51]). Such an approach is believed to alleviate the convergence issues[52] alluded to in the previous section. From an operational perspective, this transformation could be effected both in the standard Hilbert space (to be referred to as Method-I) and in the extended Hilbert space (Method-II). Nevertheless, the relative merits of the two methods and the exactness of the effective Hamiltonians derived from them deserve a through discussion. In what follows, the operational aspects of the effective Hamiltonians derived from the two methods are discussed.

A.3.1. Method-I: description in the standard Hilbert space. In the standard Hilbert space, the transformation into the CSA interaction frame is effected using the unitary transformation, U_2 ($U_2 = \exp(iH_{CSA}(t))$). As the isotropic interaction commutes with the transformation function, U_2, the isotropic part of the chemical shift interaction remains invariant.

$$\tilde{\tilde{H}}_{iso} = U_2 \tilde{H}_{iso} U_2^{-1} = \tilde{H}_{iso}. \tag{17}$$

From an experimental perspective, the form of the dipolar-coupling Hamiltonian in the CSA interaction frame remains interesting and is discussed below. In contrast to the description in the interaction frame, the static part of the dipolar-coupling Hamiltonian (say, $\tilde{H}_{D,S}$; refer to eqn (9)) in the CSA interaction frame has both a (scaled) static and time-dependent terms. In a similar vein, the time-dependent parts of the dipolar-coupling interaction in the interaction frame have additional time-dependent factors due to the CSA interactions. A detailed description of the transformed dipolar-coupling Hamiltonians is summarized by the equations given below:

$$\tilde{\tilde{H}}_{D,S} = U_2 \tilde{H}_{D,S} U_2^{-1}. \tag{18}$$

$$\tilde{\tilde{H}}_{D,S} = \left(-\frac{1}{2}\right)\left[\omega_{12}^{(-2)} e^{-i(\varphi_1(0)-\varphi_2(0))} I_1^+ I_2^- + \omega_{12}^{(2)} e^{i(\varphi_1(0)-\varphi_2(0))} I_1^- I_2^+\right]. \tag{19}$$

As illustrated above, the static part of the dipolar-coupling Hamiltonian in the CSA interaction frame has an additional (time-independent) phase factor (*i.e.*, $\varphi_n(0) = \sum_{\substack{m=-2,\\ m\neq 0}}^{2} \omega_n^{(m)} im\omega_r$) when compared to the one given in the interaction frame (refer to eqn (9)). In a similar vein, the time-dependent dipolar-coupling terms (in the interaction frame, refer to eqn (10)), get transformed as represented below:

$$\begin{aligned}\tilde{\tilde{H}}_{D,T}(t) \; &= U_2 \tilde{H}_{D,T}(t) U_2^{-1} \\ &- \left(\frac{1}{2}\right) \sum_{\substack{m=-2,\\ m\neq 2,0}}^{2} \omega_{12}^{(m)} e^{i(\varphi_1(0)-\varphi_2(0))} \sum_{k_1} b_{k_1} e^{ik_1\omega_r t} e^{im\omega_r t} I_1^+ I_2^- \\ &- \left(\frac{1}{2}\right) \sum_{\substack{m=-2,\\ m\neq 2,0}}^{2} \omega_{12}^{(m)} e^{i(\varphi_1(0)-\varphi_2(0))} \sum_{k_2} b_{k_2} e^{ik_2\omega_r t} e^{im\omega_r t} I_1^- I_2^+ \\ &+ \sum_{\substack{m=-2,\\ m\neq 0}}^{2} 2\omega_{12}^{(m)} e^{im\omega_r t} I_{1z} I_{2z}.\end{aligned} \tag{20}$$

The coefficients 'b_{k_1}', 'b_{k_2}' are derived from Bessel functions[53] and are bit complicated to evaluate. A detailed description of the procedure is described in the ESI.† As the 'b_k' coefficients constitute a product of (eight) Bessel functions, their magnitudes are significantly lower than 1.[52] Consequently, the time-dependent terms (in eqn (20)) are ignored in further discussion. Accordingly, as a first level of approximation, the effective Hamiltonian in the CSA interaction frame is represented by the equation given below:

$$\begin{aligned}H_{eff} = &\left(\omega_1^{(0)} - n\omega_r\right) I_{1z} + \left(\omega_2^{(0)} + n\omega_r\right) I_{2z} \\ &+ \left(-\frac{1}{2}\right)\left[\underbrace{\omega_{12}^{(-2)} e^{-i(\varphi_1(0)-\varphi_2(0))}}_{\omega_{12,e}^{(-2)}} I_1^+ I_2^- + \underbrace{\omega_{12}^{(2)} e^{i(\varphi_1(0)-\varphi_2(0))}}_{\omega_{12,e}^{(2)}} I_1^- I_2^+\right].\end{aligned} \tag{21}$$

To verify the exactness of the proposed effective Hamiltonians, a comparison between simulations and numerical methods is indicated in Fig. 2. As illustrated, the analytic simulations emerging from the effective Hamiltonian (refer to eqn (21)) are in good agreement, even in cases where the magnitudes of the CSA interactions are larger in comparison to the spinning frequency employed. Nevertheless, significant deviations are still observed (refer to panels (A3) and (A4) of Fig. 2) in the simulations. To resolve this issue, an alternate approach is proposed for deriving effective Hamiltonians in the CSA interaction frame.

Open Access Article. Published on 20 May 2025. Downloaded on 5/7/2026 11:37:47 PM.
This article is licensed under a Creative Commons Attribution-NonCommercial 3.0 Unported Licence.

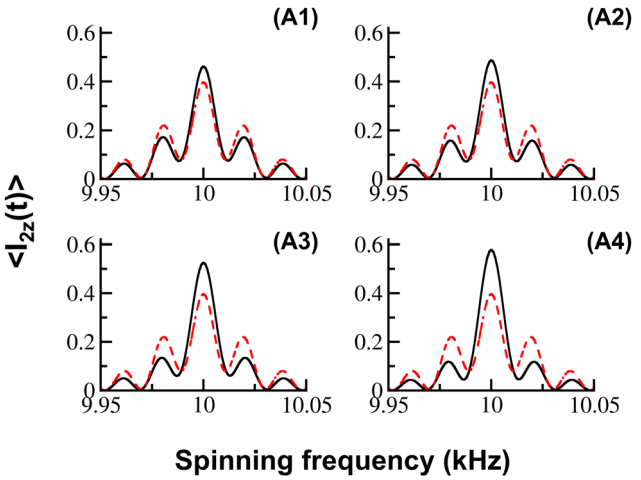

Fig. 2 In the simulations illustrated, magnetization build-up on spin 'I_2' (say, magnetization transfer from spin 'I_1' to spin 'I_2', eqn (14)) in the R^2 (corresponding to the $N = 2$ matching condition) experiment is depicted as a function of the spinning frequency. The simulations resulting from SPINEVOLUTION (indicated in black) are compared with the analytic simulations based on effective Hamiltonians in the CSA interaction frame based on eqn (21) (indicated by red broken lines). All other parameters are identical to those provided in the caption of Fig. 1.

A.3.2. Method-II: description in the extended Hilbert space. To describe the transformations in the extended Hilbert space, the time-dependent Hamiltonians in the interaction frame (eqn (5)–(7)) are transformed into a time-independent Floquet Hamiltonian.

$$H_F = \omega_r I_F + H_{iso,F} + H_{CSA,F} + H_{SD,F} + H_{TD,F}. \quad (22)$$

In the Floquet representation,[54] the time-independent terms (eqn (5) and (9)) are represented through Floquet spin operators, diagonal in the extended space, while the time-dependent terms (eqn (6) and (10)) are represented through Floquet operators, off-diagonal in the extended space. The detailed description of this procedure is well-documented[40–44] and is omitted to avoid repetition.

$$H_{iso,F} = (\omega_1^{(0)} - \omega_r)[I_{1z}]_0 + (\omega_2^{(0)} + \omega_r)[I_{2z}]_0. \quad (23)$$

$$H_{CSA,F} = \sum_{m\neq 0} G_1^{(m)}[I_{1z}]_m + \sum_{m\neq 0} G_2^{(m)}[I_{2z}]_m. \quad (24)$$

$$H_{SD,F} = \left(-\frac{1}{2}\omega_{12}^{(-2)}\right)[I_1^+ I_2^-]_0 + \left(-\frac{1}{2}\omega_{12}^{(2)}\right)[I_1^- I_2^+]_0. \quad (25)$$

$$H_{TD,F} = \sum_{m\neq 0} G_{zz}^{(m)}[I_{1z}I_{2z}]_m + \sum_{m\neq 0,-2} G_{PM}^{(m)}[I_1^+ I_2^-]_m + \sum_{m\neq 0,2} G_{MP}^{(m)}[I_1^- I_2^+]_m. \quad (26)$$

The 'G' coefficients described in the Floquet Hamiltonian are derived from the coefficients of the Hamiltonian in the interaction frame and are summarized in Table 1.

To describe the transformation into the CSA interaction frame, the Hamiltonian is initially expressed as a sum of zero-order (H_0) and perturbing terms (H_1). The perturbing Hamiltonian,

Table 1 Description of the G-coefficients along with the operators involved in the Floquet Hamiltonian H_F. The indices involved have the following values: i = 1 to 2 and the Fourier index $(m) \neq 0$

Operator	Coefficient	Operator	Coefficient
$[I_{iz}]_m$	$G_i^{(m)} = \omega_i^{(m)}$	$[I_{1z}I_{2z}]_m$	$G_{zz}^{(m)} = 2\omega_{12}^{(m)}$
$[I_1^+ I_2^-]_m$	$G_{PM}^{(m)} = -\frac{1}{2}\omega_{12}^{(m)}$	$[I_1^- I_2^+]_m$	$G_{MP}^{(m)} = -\frac{1}{2}\omega_{12}^{(m)}$

H_1, is further expressed as a sum of diagonal, $H_{1,d}$, and off-diagonal, $H_{1,od}$, terms, as illustrated below:

$$H_0 = \omega_r I_F. \quad (27)$$

$$H_{1,d} = H_{iso,F} + H_{SD,F} + H_{TD,F}. \quad (28)$$

$$H_{1,od} = H_{CSA,F}. \quad (29)$$

In contrast to the description in the standard Hilbert space, the transformation into the CSA interaction frame in the extended space is effected through the transformation function, S_1 $\left(i.e.,\ S_1 = -i\left[\sum_{m\neq 0} C_1^{(m)}[I_{1z}]_m + \sum_{m\neq 0} C_2^{(m)}[I_{2z}]_m\right]\right)$.

Accordingly, the Floquet Hamiltonian (eqn (22)) is transformed into an effective Floquet Hamiltonian, H_{eff}, as represented below.

$$H_{eff} = e^{i\lambda S_1} H_F e^{-i\lambda S_1}. \quad (30)$$

The C-coefficients in the transformation function, S_1 are chosen to compensate for the CSA interactions defined in $H_{1,od}$ ($i.e.$, $H_{1,od} = H_{CSA,F}$).

$$H_{CSA,F} + i[S_1, H_0] = 0.$$

$$\Rightarrow C_1^{(m)} = \frac{\omega_1^{(m)}}{m\omega_r} \text{ and } C_2^{(m)} = \frac{\omega_2^{(m)}}{m\omega_r}.$$

Subsequently, employing the transformation function, S_1, the various terms in $H_{1,d}$ are transformed, as given below:

$$\tilde{H}_{iso,F} = e^{i\lambda S_1} H_{iso,F} e^{-i\lambda S_1} = H_{iso,F}. \quad (31)$$

As illustrated above, the isotropic part of the chemical shift interaction remains invariant in the CSA interaction frame. This result is consistent with the description in the standard Hilbert space (refer to eqn (17)). In a similar vein, the static part of the dipolar-coupling interaction in the CSA interaction frame does get transformed into diagonal and off-diagonal terms. For illustrative purposes, we confine our discussion only to the diagonal part of the Hamiltonian in the extended space. Accordingly, the static part of the dipolar-coupling interaction in the CSA interaction frame is represented by the following

This journal is © the Owner Societies 2025

Open Access Article. Published on 20 May 2025. Downloaded on 5/7/2026 11:37:47 PM.
This article is licensed under a Creative Commons Attribution-NonCommercial 3.0 Unported Licence.

equation:

$$\tilde{H}_{\mathrm{SD,F}} = \mathrm{e}^{i\lambda S_1} H_{\mathrm{SD,F}} \mathrm{e}^{-i\lambda S_1} = \left(-\frac{1}{2}\omega_{12,e}^{(-2)}\right)\left[I_1^+ I_2^-\right]_0 + \left(-\frac{1}{2}\omega_{12,e}^{(2)}\right)\left[I_1^- I_2^+\right]_0. \quad (32)$$

The effective dipolar-coupling coefficients in the above equation have the following definitions: $\omega_{12,e}^{(-2)} = \omega_{12}^{(-2)}\cos(q)$ and $\omega_{12,e}^{(2)} = \omega_{12}^{(2)}\cos(q)$, where $q = \sqrt{2\sum_{m=1,2}\frac{\left(\omega_1^{(m)} - \omega_2^{(m)}\right)\left(\omega_1^{(-m)} - \omega_2^{(-m)}\right)}{(m\omega_r)^2}}$. While the form of the Hamiltonian in the CSA interaction frame is similar to the one derived in eqn (19), the coefficients associated with them are significantly different. As a first level of approximation, all other off-diagonal contributions emerging from the $H_{\mathrm{SD,F}}$ and $H_{\mathrm{TD,F}}$ are completely ignored in further calculations. Under the above approximation, the effective Floquet Hamiltonian in the CSA interaction frame reduces to the form given below:

$$H_{\mathrm{eff}} = \left(\omega_1^{(0)} - \omega_r\right) I_{1z} + \left(\omega_2^{(0)} + \omega_r\right) I_{2z} + \left(-\frac{1}{2}\right)\left(\omega_{12,e}^{(-2)} I_1^+ I_2^- + \omega_{12,e}^{(2)} I_1^- I_2^+\right). \quad (33)$$

To verify the exactness of the description in the extended Hilbert space, analytic simulations emerging from the effective Floquet Hamiltonian [eqn (33)] were compared with those obtained from SPINEVOLUTION.[50] As illustrated in Fig. 3, the simulations emerging from the effective Hamiltonian based on eqn (33) are in excellent agreement with those obtained from numerical methods across all regimes. From an operational perspective, the exact role of the CSA interactions (due to 'I' spins) could be deduced from the form of the two-spin effective Hamiltonian given in eqn (33). As represented, the CSA interaction scales down the dipolar-coupling coefficient (ω_{d}) and is directly responsible for the depolarization observed in systems with a large CSA interaction. In axially symmetric systems ($\eta_1 = \eta_2 = 0$) both the sign of the anisotropy parameter (δ) and the relative orientation of the CSA tensors (of the two spins I_1 and I_2) play an important role in the magnitude of the scaling factor (the '$\cos(q)$' term present in eqn (33)). In systems with positive anisotropic coefficients (δ_1, $\delta_2 > 0$), the CSA contributions become positive when CSA tensors are orthogonal to each other, contributing to the depolarization observed (the $\cos(q)$ factor decreasing) in R^2 experiments. In a similar vein, when the anisotropic coefficients are of opposite signs, the CSA contributions become additive when the CSA tensors are collinear.

Interestingly, the above predictions emerging from analytic theory are well-replicated in the simulations illustrated in Fig. 4. As illustrated, when the CSA interactions are additive (refer to panels (A2) and (A3)), the analytic simulations emerging from the effective Hamiltonians derived from the Bessel function approach (eqn (21)) are less accurate when compared to those obtained from numerical methods. By contrast, the

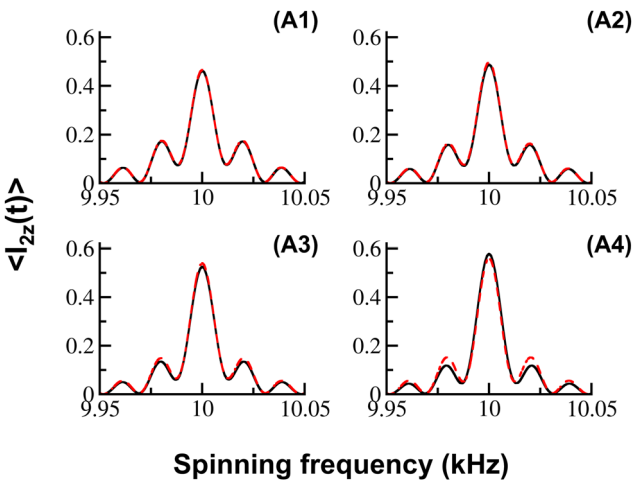

Fig. 3 In the simulations illustrated, magnetization build-up on spin 'I_2' (say, magnetization transfer from spin 'I_1' to spin 'I_2', eqn (14)) in the R^2 (corresponding to the $N = 2$ matching condition) experiment is depicted as a function of the spinning frequency. The simulations resulting from SPINEVOLUTION (indicated in black) are compared with the analytic simulations based on effective Hamiltonians in the CSA interaction frame defined in the extended Hilbert space based on eqn (33) (indicated by red broken lines). All other parameters are identical to those provided in the caption of Fig. 1.

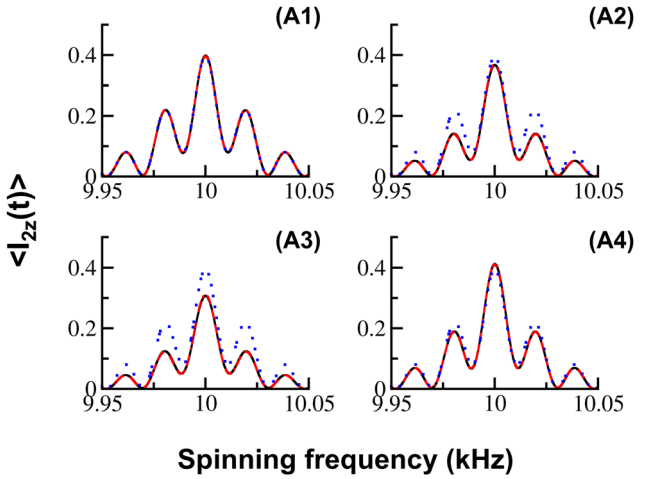

Fig. 4 In the simulations illustrated, magnetization build-up on spin 'I_2' (say, magnetization transfer from spin 'I_1' to spin 'I_2', eqn (14)) in the R^2 (corresponding to the $N = 2$ matching condition) experiment is depicted as a function of the spinning frequency. The simulations resulting from SPINEVOLUTION (indicated in black) are compared with the analytic simulations, based on Bessel formula (indicated by blue dotted lines) and effective Hamiltonians in the CSA interaction frame defined in the extended Hilbert space based on eqn (33) (red broken lines). The following specific parameters were employed in the panels: (A1) (δ_1 = 5 kHz, δ_2 = 5 kHz), (A2) (δ_1 = 5 kHz, δ_2 = 5 kHz), (A3) (δ_1 = 5 kHz, δ_2 = −5 kHz) and (A4) (δ_1 = 5 kHz, δ_2 = −5 kHz). The isotropic chemical shifts ($\omega_1^{(0)} = -\omega_2^{(0)}$ = 10 kHz), internuclear distance ($r_{I_1 I_2}$ = 3.879 Å), and mixing time (t_{mix} = 30 ms) were held constant in the simulations. For panels (A1) and (A3), the CSA parameters are $\eta_1 = 0.0$, $\Omega^{(1)} = (0^\circ, 0^\circ, 0^\circ)$; $\eta_2 = 0.0$, $\Omega^{(2)} = (0^\circ, 0^\circ, 0^\circ)$ and for panels (A2) and (A4), the CSA parameters are $\eta_1 = 0.0$, $\Omega^{(1)} = (0^\circ, 0^\circ, 0^\circ)$; $\eta_2 = 0.0$, $\Omega^{(2)} = (0^\circ, 90^\circ, 0^\circ)$. The simulations correspond to a powder sample and were implemented using 6044 orientations (zcwt6044).

Open Access Article. Published on 20 May 2025. Downloaded on 5/7/2026 11:37:47 PM.
This article is licensed under a Creative Commons Attribution-NonCommercial 3.0 Unported Licence.

analytic simulations emerging from the effective Hamiltonians (eqn (33)) defined in the extended space are in excellent agreement with those obtained from the numerical methods. In the section that follows, the dissipative effects emerging from the surrounding abundant spins is discussed in the extended Hilbert space through effective Floquet Hamiltonians.

B. Effective Hamiltonians for the system and the surroundings

As discussed in the previous section, in a real system (say, a biological sample), the ^{13}C spins are surrounded by ^{1}H spins, which are highly abundant as well as sensitive. As the ^{13}C–^{1}H dipolar-coupling interactions are stronger in magnitude when compared to the ^{13}C–^{13}C dipolar-coupling interactions, decoupling of the ^{13}C–^{1}H dipolar-coupling interactions becomes mandatory in experiments that involve measurement of ^{13}C–^{13}C distances. To minimize the contributions emerging from the ^{13}C–^{1}H dipolar-coupling interactions, strong decoupling fields are employed on the ^{1}H (proton) spins during the magnetization exchange between the ^{13}C spins. Nevertheless, residual contributions from the ^{13}C–^{1}H dipolar-coupling interactions remain and contribute to the dissipation observed in R^2 experiments. To account for this dissipation, a phenomenological damping rate constant ($1/T_{ZQ}$) is often incorporated in existing descriptions in the literature.[25–30,32–36] In the present context, this is established by including a phenomenological damping term in eqn (14), as given below.

$$\left\langle \tilde{I}_{2z}(t) \right\rangle = \exp\left(-\frac{t}{T_{ZQ}}\right)\frac{{\omega_d}^2}{(\Omega^2+{\omega_d}^2)}\sin^2\left(\sqrt{(\Omega^2+{\omega_d}^2)}\right)t. \quad (34)$$

While the above description (or model) of the spin dynamics is conceptually flawed,[37] a lack of alternate theoretical models has encouraged the use of other experiments[55–60] for providing a qualitative estimate of homonuclear distances in solids abandoning the need for accurate measurements. The implications of this conceptual digression are beyond the scope of this article.

From a theoretical perspective, the dissipation (or depolarization) observed on the system of interest (say, spins I_1 and I_2) resulting from its coupling to the surrounding environment or bath (say, abundant 'S' spins) is studied using the following general equation.

$$H(t) = H_{System}(t) + H_{Bath}(t) + H_{System-Bath}(t). \quad (35)$$

The interactions of the observed spins (say, I_1 and I_2) are contained in the system Hamiltonian, $H_{System}(t)$ (similar to eqn (1)). In the present context, the bath Hamiltonian comprises the chemical shift and the homonuclear dipolar interactions in addition to the decoupling field employed.

$$H_{Bath}(t) = H_S(t) + H_{RF} \quad (36)$$

where,

$$\begin{aligned} H_S(t) &= \sum_{j=1}^{N}\omega_j^{(0)}S_{jz} + \sum_{\substack{m=-2,\\ m\neq 0}}^{2}\sum_{j=1}^{N}\omega_j^{(m)}e^{im\omega_r t}S_{jz} \\ &+ \sum_{\substack{m=-2,\\ m\neq 0}}^{2}\sum_{j<k=1}^{N}\omega_{jk}^{(m)}e^{im\omega_r t}\left[2S_{jz}S_{kz} + \left(-\frac{1}{2}\right)\right. \\ &\left.\times\left(S_j^+S_k^- + S_j^-S_k^+\right)\right], \end{aligned} \quad (37)$$

and

$$H_{RF} = \omega_{rf}\sum_{j=1}^{N}S_{jx}. \quad (38)$$

A detailed description of the coefficients employed in the above equations is given in the ESI.†

The interaction between the system and the bath is depicted through the heteronuclear dipolar interactions and is represented by $H_{System-Bath}(t)$.

$$H_{System-Bath}(t) = \sum_{\substack{m=-2,\\ m\neq 0}}^{2}\sum_{i=1}^{2}\sum_{j=1}^{N}\omega_{ij}^{(m)}e^{im\omega_r t}(2I_{iz}S_{jz}). \quad (39)$$

From an operational perspective, the solution to the quantum-Liouville equation (eqn (4a)) becomes quite complicated due to the time-dependent coefficients as well as the increased dimensionality of the problem (dimension is given by $(2I_1+1)(2I_2+1)\prod_{i=1}^{N}(2S_i+1)$). Hence, phenomenological models (employing exponential damping terms) have been integrated within a two-spin framework.

As an alternative, below we present an analytic formulation for describing the dissipative effects observed in R^2 experiments. In the proposed approach, effective Floquet Hamiltonians (defined in the CSA interaction frame of the ^{13}C-spins) are derived for describing the spin dynamics in the presence of protons under heteronuclear decoupling. A detailed description of the calculations within the Floquet framework is summarized in the ESI.† In contrast to the description based on the effective Hamiltonians in the interaction frame,[41] the present framework affords a spin dynamical description in the CSA interaction frame and facilitates studies even in systems with larger chemical shift anisotropies. For illustrative purposes, the multi-spin effects observed in R^2 experiments are described through models (comprising a finite number of spins) based on effective Floquet Hamiltonians.

B.1. Three-spin model (I_1I_2S or ^{13}C–^{13}C–^{1}H). Based on the theoretical description in the ESI,† the effective Hamiltonian (comprising three spins) describing the spin dynamics is

 This journal is © the Owner Societies 2025

Open Access Article. Published on 20 May 2025. Downloaded on 5/7/2026 11:37:47 PM.
This article is licensed under a Creative Commons Attribution-NonCommercial 3.0 Unported Licence.

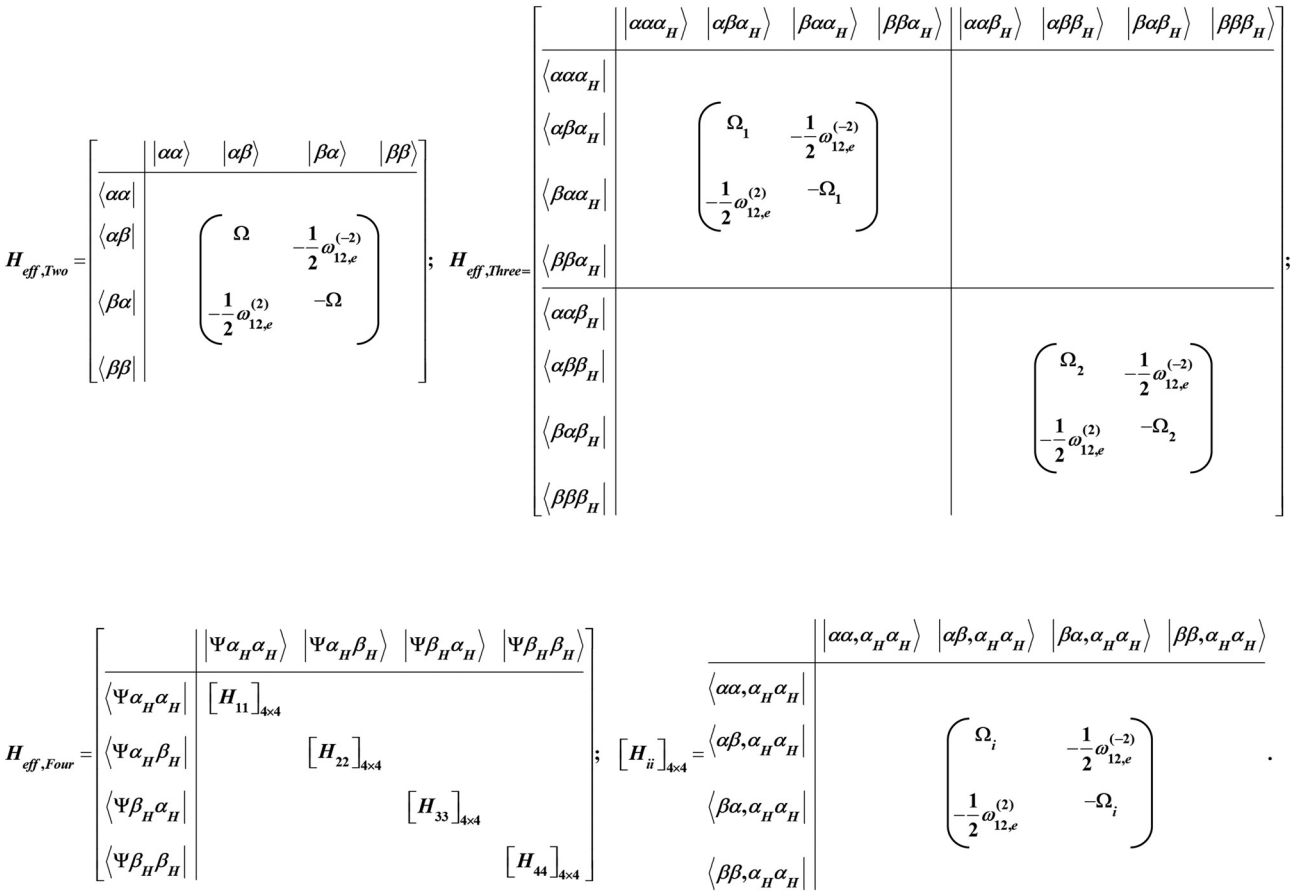

Fig. 5 Representation of the effective Hamiltonian in the model two-, three-, and four-spin systems in the block-diagonal form (of 2 × 2 matrices).

represented by the following equation.

$$H_{\text{eff}} = \left(\omega_1^{(0)} - n\omega_r\right) I_{1z} + \left(\omega_2^{(0)} + n\omega_r\right) I_{2z} + \left(-\frac{1}{2}\right)\left[\omega_{12,e}^{(-2)} I_1^+ I_2^- + \omega_{12,e}^{(2)} I_1^- I_2^+\right] + d_1 I_{1z} S_z + e_1 I_{2z} S_z. \tag{40}$$

The coefficients 'd_1' and 'e_1' represent the residual heteronuclear dipolar-coupling interactions (due to cross terms between the ^{1}H-CSA interaction and ^{13}C–^{1}H heteronuclear dipolar interactions) associated with the spins, I_1 and I_2, respectively. Accordingly, in the presence of a single 'S'-spin (say, ^{1}H-spin), the effective Hamiltonian (of dimension 8 × 8) is decomposed into two two-level systems (TLSs) (refer to Fig. 5) and the magnetization transfer between the spins I_1 and I_2 is described by two oscillatory functions given below:

$$\langle \tilde{I}_{2z}(t)\rangle = \underbrace{\left(\frac{1}{2}\right)\frac{{\omega_{\text{d}}}^2}{({\Omega_1}^2 + {\omega_{\text{d}}}^2)}\sin^2\left(\sqrt{({\Omega_1}^2 + {\omega_{\text{d}}}^2)}\right)t}_{\alpha-\text{state of } S-\text{spin}} + \underbrace{\left(\frac{1}{2}\right)\frac{{\omega_d}^2}{({\Omega_2}^2 + {\omega_d}^2)}\sin^2\left(\sqrt{({\Omega_2}^2 + {\omega_d}^2)}\right)t}_{\beta-\text{state of } S-\text{spin}} \tag{41}$$

The factor $\left(\frac{1}{2}\right)$ in the trigonometric expression represents the normalization factor and could be related to the number of spin states of the 'S'-spin (say, ^{1}H). This factoring of the result could also be deduced from the matrix representation of the effective Hamiltonians depicted in Fig. 5.

In contrast to the isolated two-spin model (refer to eqn (14)), the effective offset term (denoted by Ω) experienced by spins I_1 and I_2 comprises additional contributions from the residual heteronuclear dipolar-coupling interactions and is primarily responsible for the increased dissipation observed in the presence of a single proton. A detailed description of the effective offset, Ω, is summarized in Table 2. In contrast to the constant dissipative term, T_{2Q}, introduced in eqn (34), the dissipation due to Ω is orientation-dependent. To verify the exactness of the above analytic expression, simulations in the model dipeptide *N*-acetyl-L-valine-L-leucine (VL)[61] were employed as a model system in the present study. The above choice of the model system is only for demonstrative purposes and has nothing to do with the suitability of the theoretical framework presented in this report.

To demonstrate the dissipative effects emerging from protons, the magnetization exchange between the ^{13}C spins (say, V_{CO} and $V_{C\gamma 1}$, corresponding to a distance of 3.879 Å) was examined in the presence of different protons (say, H_α, H_β and

Open Access Article. Published on 20 May 2025. Downloaded on 5/7/2026 11:37:47 PM.
This article is licensed under a Creative Commons Attribution-NonCommercial 3.0 Unported Licence.

Table 2 Description of the dissipative terms employed in various multi-spin systems

Spin systems	Offset, Ω	Coefficients
I_1–I_2	Ω	$\frac{1}{2}\left(\omega_1^{(0)} - \omega_2^{(0)} - 2\omega_r\right)$
I_1–I_2–S	Ω_1	$\frac{1}{2}\left(\omega_1^{(0)} - \omega_2^{(0)} - 2\omega_r\right) + \frac{1}{4}(d_1 - e_1)$
	Ω_2	$\frac{1}{2}\left(\omega_1^{(0)} - \omega_2^{(0)} - 2\omega_r\right) - \frac{1}{4}(d_1 - e_1)$
I_1–I_2–S_1–S_2	Ω_1	$\frac{1}{2}\left(\omega_1^{(0)} - \omega_2^{(0)} - 2\omega_r\right) + \frac{1}{4}(d_1 - e_1) + \frac{1}{4}(d_2 - e_2)$
	Ω_2	$\frac{1}{2}\left(\omega_1^{(0)} - \omega_2^{(0)} - 2\omega_r\right) + \frac{1}{4}(d_1 - e_1) - \frac{1}{4}(d_2 - e_2)$
	Ω_3	$\frac{1}{2}\left(\omega_1^{(0)} - \omega_2^{(0)} - 2\omega_r\right) - \frac{1}{4}(d_1 - e_1) + \frac{1}{4}(d_2 - e_2)$
	Ω_4	$\frac{1}{2}\left(\omega_1^{(0)} - \omega_2^{(0)} - 2\omega_r\right) - \frac{1}{4}(d_1 - e_1) - \frac{1}{4}(d_2 - e_2)$
I_1–I_2–S_1–S_2–S_3	Ω_1	$\frac{1}{2}\left(\omega_1^{(0)} - \omega_2^{(0)} - 2\omega_r\right) + \frac{1}{4}(d_1 - e_1) + \frac{1}{4}(d_2 - e_2) + \frac{1}{4}(d_3 - e_3)$
	Ω_2	$\frac{1}{2}\left(\omega_1^{(0)} - \omega_2^{(0)} - 2\omega_r\right) + \frac{1}{4}(d_1 - e_1) + \frac{1}{4}(d_2 - e_2) - \frac{1}{4}(d_3 - e_3)$
	Ω_3	$\frac{1}{2}\left(\omega_1^{(0)} - \omega_2^{(0)} - 2\omega_r\right) + \frac{1}{4}(d_1 - e_1) - \frac{1}{4}(d_2 - e_2) + \frac{1}{4}(d_3 - e_3)$
	Ω_4	$\frac{1}{2}\left(\omega_1^{(0)} - \omega_2^{(0)} - 2\omega_r\right) + \frac{1}{4}(d_1 - e_1) - \frac{1}{4}(d_2 - e_2) - \frac{1}{4}(d_3 - e_3)$
	Ω_5	$\frac{1}{2}\left(\omega_1^{(0)} - \omega_2^{(0)} - 2\omega_r\right) - \frac{1}{4}(d_1 - e_1) + \frac{1}{4}(d_2 - e_2) + \frac{1}{4}(d_3 - e_3)$
	Ω_6	$\frac{1}{2}\left(\omega_1^{(0)} - \omega_2^{(0)} - 2\omega_r\right) - \frac{1}{4}(d_1 - e_1) + \frac{1}{4}(d_2 - e_2) - \frac{1}{4}(d_3 - e_3)$
	Ω_7	$\frac{1}{2}\left(\omega_1^{(0)} - \omega_2^{(0)} - 2\omega_r\right) - \frac{1}{4}(d_1 - e_1) - \frac{1}{4}(d_2 - e_2) + \frac{1}{4}(d_3 - e_3)$
	Ω_8	$\frac{1}{2}\left(\omega_1^{(0)} - \omega_2^{(0)} - 2\omega_r\right) - \frac{1}{4}(d_1 - e_1) - \frac{1}{4}(d_2 - e_2) - \frac{1}{4}(d_3 - e_3)$

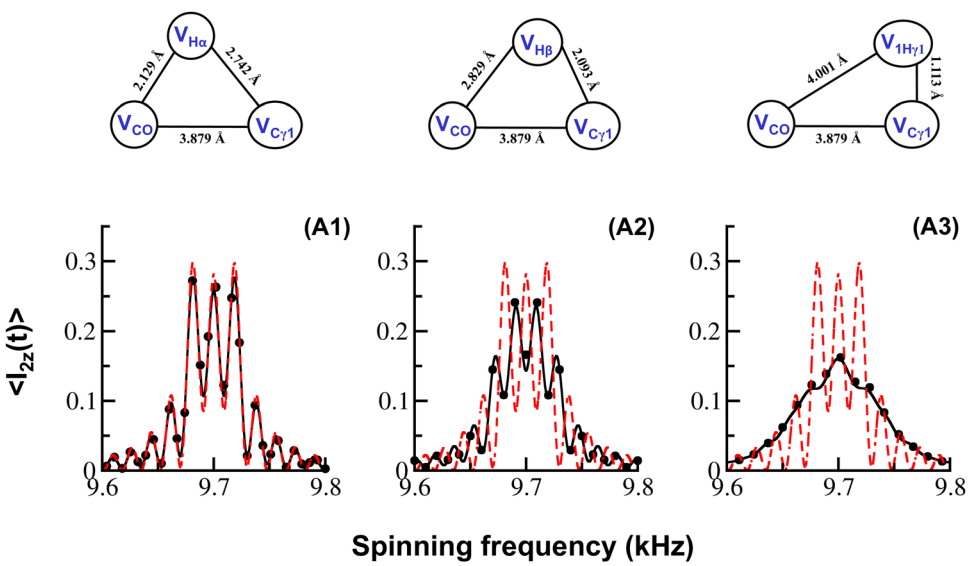

Fig. 6 In the three-spin simulations illustrated, magnetization build-up on spin 'I_2' (say, magnetization transfer from spin 'I_1' to spin 'I_2', eqn (41)) in the R^2 (corresponding to the N = 2 matching condition) experiment is depicted as a function of the spinning frequency. The simulations resulting from SPINEVOLUTION (indicated in black) are compared with the analytic three-spin simulations based on eqn (41) (indicated by black dots). The simulations depicted in the panels correspond to the following model systems: (A1) – $V_{CO}V_{C\gamma1}V_{H\alpha}$, (A2) – $V_{CO}V_{C\gamma1}V_{H\beta}$, and (A3) – $V_{CO}V_{C\gamma1}V_{1H\gamma1}$. Analytic simulations emerging from the isolated two-spin model (V_{CO}–$V_{C\gamma1}$) are indicated by red broken lines in the backdrop. Information about all the simulation parameters employed in the simulations is given in Table S2 in the ESI.†

This journal is © the Owner Societies 2025

Open Access Article. Published on 20 May 2025. Downloaded on 5/7/2026 11:37:47 PM.
This article is licensed under a Creative Commons Attribution-NonCommercial 3.0 Unported Licence.

$H_{\gamma 1}$ in the valine residue). As depicted in the simulations (refer to Fig. 6), the simulations emerging from eqn (41) (indicated in black dots) are in excellent agreement with those obtained from SPINEVOLUTION (indicated by solid black lines). For comparative purposes, the simulations emerging from the isolated two-spin model are also indicated (by red broken lines) in the backdrop. As depicted, the dissipative effect is significant (see panel (A3)) in systems with stronger heteronuclear dipolar-coupling interactions (say, between ^{13}C–^{1}H in the present case). A detailed description of the parameters employed is summarized in the ESI.† Hence, as the number of proton spins increases in the system, the dissipative effects should in principle increase and are verified below employing four- and five-spin model systems.

B.2. Four-spin model ($I_1I_2S_1S_2$ or ^{13}C–^{13}C–^{1}H–^{1}H). Following the theoretical description (presented in the ESI†), the effective Hamiltonian for the model four-spin system (comprising two carbons and two protons) is derived and represented below.

$$\begin{aligned} H_{\text{eff}} &= \left(\omega_1^{(0)} - n\omega_r\right)I_{1z} + \left(\omega_2^{(0)} + n\omega_r\right)I_{2z} \\ &+ \left(-\frac{1}{2}\right)\left[\omega_{12,e}^{(-2)}I_1^+I_2^- + \omega_{12,e}^{(2)}I_1^-I_2^+\right] \\ &+ \sum_{i=1}^{2} d_i I_{1z}S_{iz} + \sum_{i=1}^{2} e_i I_{2z}S_{iz}. \end{aligned} \tag{42}$$

Analogous to the three-spin problem, the effective Hamiltonian for the above four-spin system (described by a 16 × 16 matrix) is block-diagonal and could be expressed in terms of four TLSs (refer to Fig. 5). Consequently, the magnetization transfer between spins I_1 and I_2 in the presence of two S-spins (say, S_1 and S_2) is described in terms of the four oscillatory functions given below.

$$\begin{aligned} \langle \tilde{I}_{2z}(t)\rangle &= \underbrace{\left(\frac{1}{4}\right)\frac{\omega_d^2}{(\Omega_1^2+\omega_d^2)}\sin^2\left(\sqrt{(\Omega_1^2+\omega_d^2)}\right)t}_{\alpha\alpha\text{-state of } S\text{-spin}} \\ &+ \underbrace{\left(\frac{1}{4}\right)\frac{\omega_d^2}{(\Omega_2^2+\omega_d^2)}\sin^2\left(\sqrt{(\Omega_2^2+\omega_d^2)}\right)t}_{\alpha\beta\text{-state of } S\text{-spin}} \\ &+ \underbrace{\left(\frac{1}{4}\right)\frac{\omega_d^2}{(\Omega_3^2+\omega_d^2)}\sin^2\left(\sqrt{(\Omega_3^2+\omega_d^2)}\right)t}_{\beta\alpha\text{-state of } S\text{-spin}} \\ &+ \underbrace{\left(\frac{1}{4}\right)\frac{\omega_d^2}{(\Omega_4^2+\omega_d^2)}\sin^2\left(\sqrt{(\Omega_4^2+\omega_d^2)}\right)t}_{\beta\beta\text{-state of } S\text{-spin}}. \end{aligned} \tag{43}$$

In line with the discussion presented in the three-spin model, four oscillatory functions could be associated with the four spin states of the two protons considered. In the simulations depicted in Fig. 7, the magnetization transfer between spins I_1 and I_2 is described in the presence of two 'S' spins. As illustrated, the analytic simulations based on eqn (43) are in good agreement and validate the theoretical model presented above. In contrast to the three-spin simulations, the dissipative

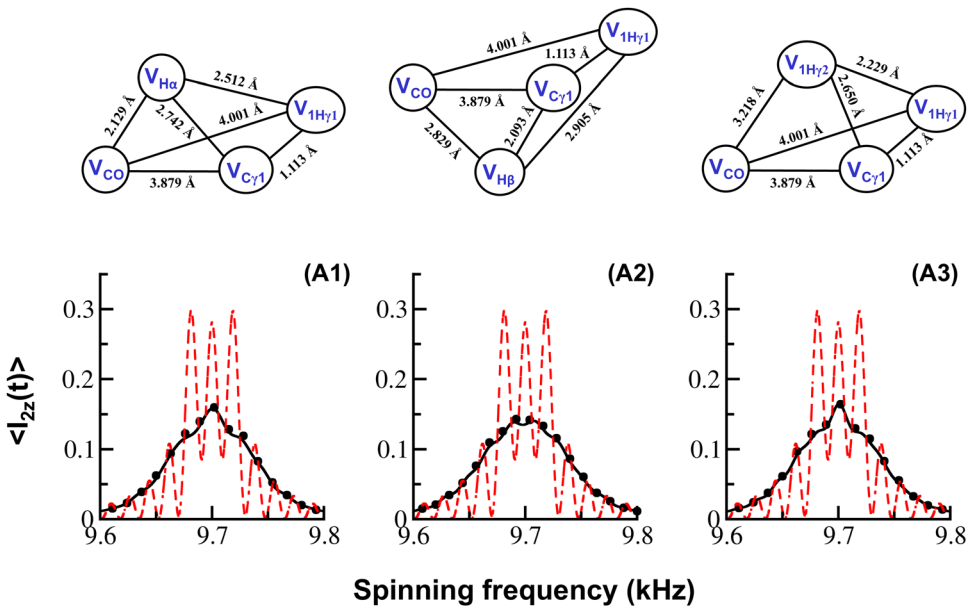

Fig. 7 In the four-spin simulations illustrated, magnetization build-up on spin 'I_2' (say, magnetization transfer from spin 'I_1' to spin 'I_2', eqn (43)) in the R^2 (corresponding to the N = 2 matching condition) experiment is depicted as a function of the spinning frequency. The simulations resulting from SPINEVOLUTION (indicated in black) are compared with the analytic simulations based on eqn (43) (indicated by black dots). The simulations depicted in the panels correspond to the following model systems: (A1) – $V_{CO}V_{C\gamma 1}V_{H\alpha}V_{1H\gamma 1}$, (A2) – $V_{CO}V_{C\gamma 1}V_{H\beta}V_{1H\gamma 1}$, and (A3) – $V_{CO}V_{C\gamma 1}V_{1H\gamma 1}V_{1H\gamma 2}$. Analytic simulations emerging from the isolated two-spin model (V_{CO}–$V_{C\gamma 1}$) are indicated by red broken lines in the backdrop. The parameters employed in the simulations are given in Table S2 in the ESI.†

Open Access Article. Published on 20 May 2025. Downloaded on 5/7/2026 11:37:47 PM.
This article is licensed under a Creative Commons Attribution-NonCommercial 3.0 Unported Licence.

effects are significant in the four-spin system and are well-validated in the analytic simulations.

B.3. Five-spin model ($I_1I_2S_1S_2S_3$ or ^{13}C–^{13}C–^{1}H–^{1}H–^{1}H). To further substantiate the validity of the analytic method, magnetization transfer between the two '*I*-spins' was also examined in the presence of three '*S*'-spins. The underlying equations depicting the magnetization transfer are summarized below.

$$H_{\text{eff}} = \left(\omega_1^{(0)} - n\omega_r\right)I_{1z} + \left(\omega_2^{(0)} + n\omega_r\right)I_{2z} + \left(-\frac{1}{2}\right)\left[\omega_{12,e}^{(-2)}I_1^+I_2^- + \omega_{12,e}^{(2)}I_1^-I_2^+\right] + \sum_{i=1}^{3} d_iI_{1z}S_{iz} + \sum_{i=1}^{3} e_iI_{2z}S_{iz}. \quad (44)$$

$$\langle \tilde{I}_{2z}(t)\rangle = \left(\frac{1}{2^N}\right)\sum_{i=1}^{2^N}\frac{{\omega_d}^2}{(\Omega_i^2+\omega_d^2)}\sin^2\left(\sqrt{(\Omega_i^2+\omega_d^2)}\right)t \quad (N=3). \quad (45)$$

As illustrated above, magnetization transfer in the model five-spin system is described by eight oscillatory functions (corresponding to eight different terms, represented by Ω_i). A brief summary of the dissipative terms is summarized in Table 2. In accord with eqn (41) and (43), the normalization factor, $(1/2^N)$, depends on the number of spins (say, *S*-spins) coupled to the spin system of interest (say, I_1 and I_2).

To elucidate the role of protons, magnetization transfer in the weak-coupling regime was also examined in the simulations depicted in Fig. 8.

As depicted through the simulations illustrated in Fig. 6–8, the depolarization effects observed in magnetization exchange experiments (between spins I_1 and I_2) is largely influenced by the spin topology of the system under consideration. In contrast to other existing descriptions, the spin dynamics in a multi-spin system are described in a reduced subspace (spanned by 2 × 2 matrices) resulting in simple trigonometric expressions analogous to the one obtained in the description of an isolated two-spin system. As illustrated in the above examples, depending on the number of '*S*' spins coupled to the system of interest, the polarization transfer from spin I_1 to I_2 in a model I_1–I_2–S_N system is described in terms of simple trigonometric expressions emerging from 2^N two-level systems (TLSs). Such an approach is computationally robust and presents an attractive framework for estimating multiple anisotropic constraints (such as ^{13}C–^{13}C, ^{13}C–^{1}H dipolar information besides the orientation and magnitude of the chemical shift and dipolar tensors). When the spinning frequency (based on the chemical shift difference between spins I_1 and I_2) is lower

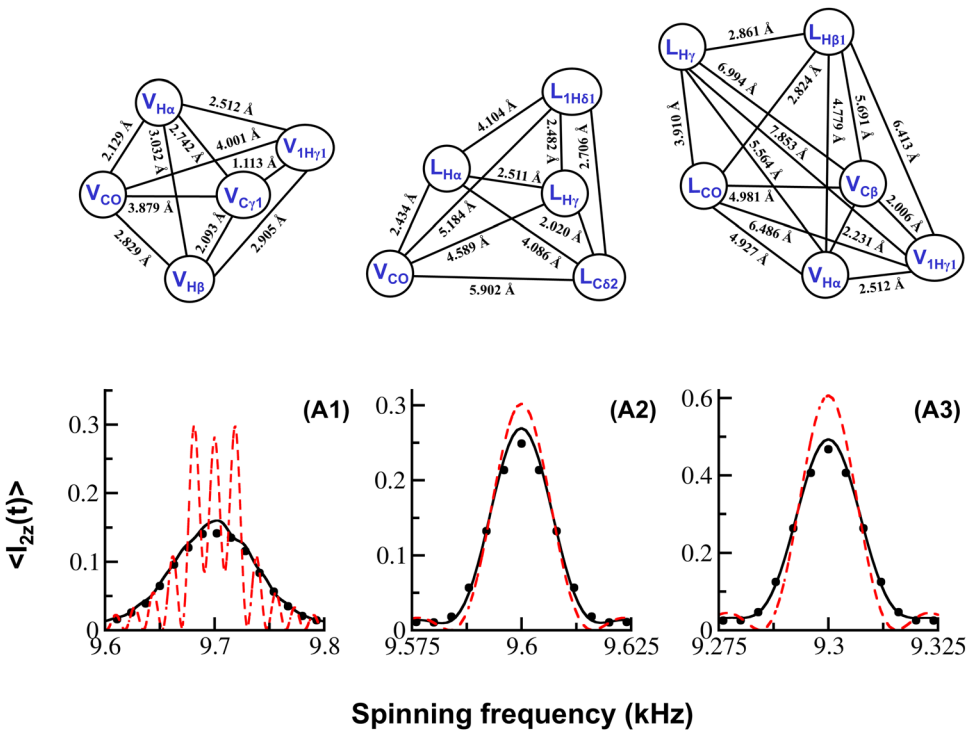

Fig. 8 In the simulations illustrated, magnetization build-up on spin 'I_2' (say, magnetization transfer from spin 'I_1' to spin 'I_2', eqn (45)) in the R^2 (corresponding to the N = 2 matching condition) experiment is depicted as a function of the spinning frequency. The simulations resulting from SPINEVOLUTION (indicated in black) are compared with the analytic simulations based on eqn (45) (indicated by black dots). The simulations depicted in the panels correspond to the following model systems: panel (A1) – $V_{CO}V_{C\gamma1}V_{H\alpha}V_{H\beta}V_{1H\gamma1}$, panel (A2) – $V_{CO}L_{C\delta2}L_{H\alpha}L_{H\gamma}L_{1H\delta1}$, and panel (A3) – $L_{CO}V_{C\beta}V_{H\alpha}V_{1H\gamma1}L_{H\beta1}L_{H\gamma}$. Analytic simulations emerging from the isolated two-spin model are indicated (panel (A1) – $V_{CO}V_{C\gamma1}$, r = 3.879 Å, panel (A2) – $V_{CO}L_{C\delta}2$, r = 5.902 Å, and panel (A3) – $L_{CO}V_{C\beta}$, r = 4.981 Å) by red broken lines in the backdrop. The parameters employed in the simulations are given in Table S2 in the ESI.†

 This journal is © the Owner Societies 2025

Open Access Article. Published on 20 May 2025. Downloaded on 5/7/2026 11:37:47 PM.
This article is licensed under a Creative Commons Attribution-NonCommercial 3.0 Unported Licence.

than the magnitude of the CSA interactions (of the observed spins),[62] the CSA interaction coefficients play a prominent role in scaling down the recoupled dipolar-coupling constant and are directly responsible for decreasing the efficiency of polarization transfer, even in an isolated coupled system.

By contrast, the CSA interactions of the unobserved/decoupled spins (say, 'S' spins) play an active role in the dissipative effects emanating from the coupling to the neighboring 'S' spins. In the present context, the depolarization effects are manifested through the offset terms, Ω_i, and have contributions from (i) the isotropic chemical shifts of the observed spins (I_1 and I_2), and (ii) the cross terms between the (transverse components) CSA interactions of the unobserved spins (say, 'S' spins) and the (transverse components) residual heteronuclear dipolar interactions

$$(i.e., \left[\underbrace{S_{\pm}}_{\text{CSA}}, \underbrace{I_z S_{\mp}}_{\substack{\text{Heteronuclear}\\ \text{dipolar}}}\right] = I_z S_z).$$

When the CSA interactions associated with the 'S' spins are absent (or compensated for through multiple pulse-based methods), the depolarization effects emerging from the residual couplings to the 'S' spins should vanish (in principle), thereby reducing the spin dynamics to that of an isolated two-spin system. This prediction emerging from the analytic theory is well-substantiated through the simulations given in Fig. 9. As illustrated in Fig. 9, in the absence of the CSA interactions (of the S-spins), the simulations from the multi-spin model system, I_1–I_2–S_N (depicted in Fig. 8), reduce to that of an isolated two-spin system (I_1–I_2). Hence, compensating for the effects of the CSA interactions of the decoupled spins plays an important role in improving the efficiency of magnetization transfer among spins in R^2 experiments.

Besides its implications in quantifying the R^2 experiments, the proposed analytic model (trigonometric expressions) also offers a framework for describing magnetization transfer among spins (I_1 and I_2) induced by multiple-pulse-based dipolar recoupling experiments. From an operational perspective, the only difference arises from the scaling factors associated with the coefficients 'ω_d' and 'Ω_i' employed in eqn (13) and (14). Depending on the desired applications, multiple-pulse experiments are designed to scale down both the anisotropic interactions (such as dipolar and CSA interactions) as well as the isotropic chemical shift interactions of interest. Hence, the proposed framework is well-suited to describe polarization transfer in I_1–I_2–S_N systems both in the presence and absence of multiple pulses. We believe that the theoretical framework presented in this article would benefit in the analysis of longitudinal relaxation times measured under R^2 conditions and its potential in other related areas.[62]

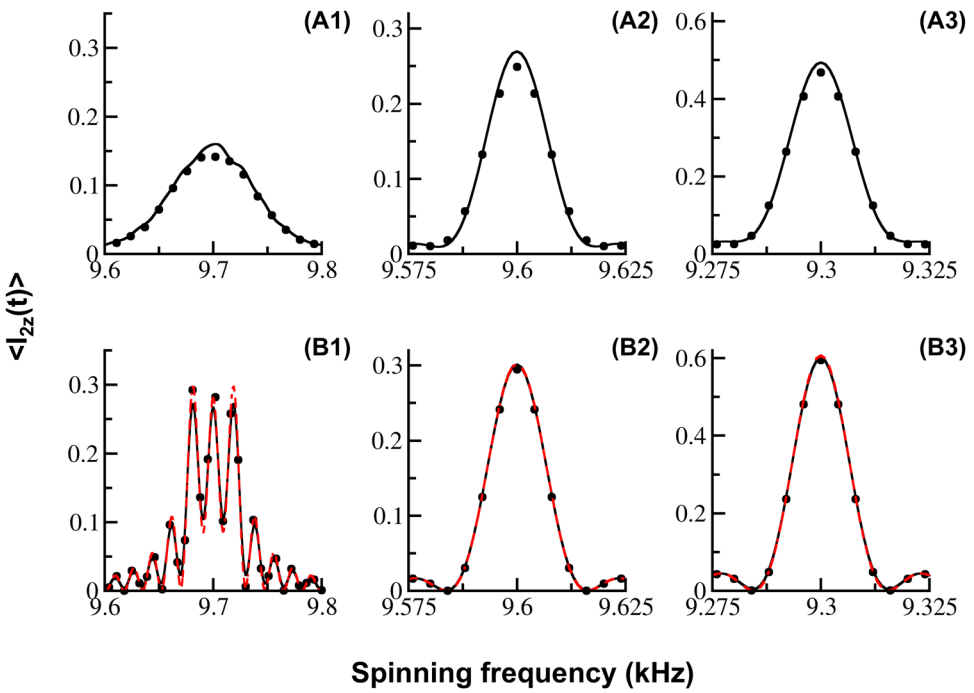

Fig. 9 In the simulations illustrated, magnetization build-up on spin 'I_2' (say, magnetization transfer from spin 'I_1' to spin 'I_2', eqn (45)) in the R^2 (corresponding to the N = 2 matching condition) experiment is depicted as a function of the spinning frequency in both the presence (refer to panels (A1)–(A3)) and absence (refer to panels (B1)–(B3)) of the CSA interactions of proton spins. The simulations resulting from SPINEVOLUTION (indicated in black) are compared with the analytic simulations based on eqn (45) (indicated by black dots). The simulations depicted in the panels correspond to the following model systems: panels (A1) and (B1) – $V_{CO}V_{C\gamma 1}V_{H\alpha}V_{H\beta}V_{1H\gamma 1}$, panels (A2) and (B2) – $V_{CO}L_{C\delta 2}L_{H\alpha}L_{H\gamma}L_{1H\delta 1}$, and panels (A3) and (B3) – $L_{CO}V_{C\beta}V_{H\alpha}V_{1H\gamma 1}L_{H\beta 1}L_{H\gamma}$. Analytic simulations emerging from the isolated two-spin model are indicated (panel (B1) – $V_{CO}V_{C\gamma 1}$, r = 3.879 Å, panel (B2) – $V_{CO}L_{C\delta}2$, r = 5.902 Å, and panel (B3) – $L_{CO}V_{C\beta}$, r = 4.981 Å) by red broken lines in the backdrop. The parameters employed in the simulations are given in Table S2 in the ESI.†

Open Access Article. Published on 20 May 2025. Downloaded on 5/7/2026 11:37:47 PM. This article is licensed under a Creative Commons Attribution-NonCommercial 3.0 Unported Licence.

As evident from the present framework, the CSA interactions of the observed spins (say, '*I*' spins) directly scale the estimated dipolar coupling, while the CSA interactions of the unobserved/decoupled spins (say, '*S*' spins) directly contribute to the residual dipolar-coupling interactions leading to different offset terms Ω_i. This directly results in different trigonometric terms and is directly responsible for the dissipation observed in the R^2 experiments.

III. Conclusions and perspectives

In summary, the present study explicates the exact role of chemical shift anisotropic spin interactions in magnetization exchange between spins observed in R^2 experiments. From the proposed theoretical framework, the dissipation (or dissipative effects) observed in R^2 experiments could be explained in terms of both the (i) scaling factors associated with the measured dipolar-coupling constant (between the '*I*' spins) and (ii) effective offset term (Ω_i) experienced by spins I_1 and I_2. The scaling factor associated with the dipolar-coupling constant is derived in terms of effective Hamiltonians defined in the CSA interaction frame (defined by the '*I*-spins'). By contrast, the CSA interactions of the unobserved (abundant) spins play an important role in the effective offset (Ω_i) experienced by the spins, I_1 and I_2. In the effective Hamiltonian framework, the cross terms between the CSA interactions (of the abundant ^{1}H's) and the heteronuclear dipolar-coupling interactions (say, ^{13}C–^{1}H) result in two-spin longitudinal operators, I_zS_z. This, in turn, contributes to the offset experienced by the spins, I_1 and I_2. Depending on the number of *S*-spins, the number of trigonometric functions increases and is directly responsible for the dissipation observed in magnetization exchange experiments between spins I_1 and I_2 in R^2 experiments. Hence, the CSA interactions of the *S*-spins play an important role in the dissipation observed in the R^2 experiments. In contrast to (existing) phenomenological models, the dissipation observed in R^2 experiments is orientation-dependent and has a profound dependence on the dipolar coupling and CSA parameters of the unobserved *S*-spins. Additionally, the trigonometric expressions derived from the proposed analytic method present an attractive framework for estimating the dipolar-coupling constant and CSA parameters of the observed spins (I_1, I_2) in addition to estimating the coupling constant associated with the heteronuclear dipolar-coupling interactions (say, ^{13}C–^{1}H).

Data availability

Data sharing is not applicable to paper as no data were created or analyzed in this study.

Conflicts of interest

The authors declare that they have no known competing financial interests or personal relationships that could have appeared to influence the work reported in this paper.

Acknowledgements

N. S. would like to thank IIT Ropar for the graduate assistantship. M. K. P. would like to acknowledge IIT Ropar for the research infrastructure.

References

1 Y. Nishiyama, G. Hou, V. Agarwal, Y. Su and A. Ramamoorthy, Ultrafast magic angle spinning solid-state NMR spectroscopy: advances in methodology and applications, *Chem. Rev.*, 2023, **123**, 918–988.
2 B. Reif, S. E. Ashbrook, L. Emsley and M. Hong, Solid-state NMR spectroscopy, *Nat. Rev. Methods Primers*, 2021, **1**, 2.
3 Z. J. Berkson, S. Bjorgvinsdottir, A. Yakimov, D. Gioffre, M. D. Korzynski, A. B. Barnes and C. Coperet, Solid-state NMR spectra of protons and quadrupolar nuclei at 28.2 T: resolving signatures of surface sites with fast magic angle spinning, *JACS Au*, 2022, **2**, 2460–2465.
4 A. A. Smith, M. Ernst, S. Riniker and B. H. Meier, Localized and collective motions in HETs (218–289) fibrils from combined NMR relaxation and MD simulation, *Angew. Chem.*, 2019, **131**, 9483–9488.
5 R. Zhang, K. H. Mroue and A. Ramamoorthy, Proton-based ultrafast magic angle spinning solid-state NMR spectroscopy, *Acc. Chem. Res.*, 2017, **50**, 1105–1113.
6 D. Good, C. Pham, J. Jagas, J. R. Lewandowski and V. Ladizhansky, Solid-state NMR provides evidence for small-amplitude slow domain motions in a multispanning transmembrane α-helical protein, *J. Am. Chem. Soc.*, 2017, **139**, 9246–9258.
7 S. J. Opella, Solid-state NMR and membrane proteins, *J. Magn. Reson.*, 2015, **253**, 129–137.
8 S. Wang and V. Ladizhansky, Recent advances in magic angle spinning solid state NMR of membrane proteins, *Prog. Nucl. Magn. Reson. Spectrosc.*, 2014, **82**, 1–26.
9 E. R. Andrew, A. Bradbury and R. G. Eades, Nuclear magnetic resonance spectra from a crystal rotated at high speed, *Nature*, 1958, **182**, 1659.
10 I. J. Lowe, Free induction decays of rotating solids, *Phys. Rev. Lett.*, 1959, **2**, 285–287.
11 Y. Nishiyama, Fast magic-angle sample spinning solid-state NMR at 60–100 kHz for natural abundance samples, *Solid State Nucl. Magn. Reson.*, 2016, **78**, 24–36.
12 K. Takeda, Microcoils and microsamples in solid-state NMR, *Solid State Nucl. Magn. Reson.*, 2012, **47–48**, 1–9.
13 Y. K. Lee, N. D. Kurur, M. Helmle, O. G. Johannessen, N. C. Nielsen and M. H. Levitt, Efficient dipolar recoupling in the NMR of rotating solids. a sevenfold symmetric radio-frequency pulse sequence, *Chem. Phys. Lett.*, 1995, **242**, 304–309.
14 M. Hohwy, H. J. Jakobsen, M. Edén, M. H. Levitt and N. C. Nielsen, Broadband dipolar recoupling in the nuclear magnetic resonance of rotating solids: a compensated c7 pulse sequence, *J. Chem. Phys.*, 1998, **108**, 2686–2694.

Open Access Article. Published on 20 May 2025. Downloaded on 5/7/2026 11:37:47 PM.
This article is licensed under a Creative Commons Attribution-NonCommercial 3.0 Unported Licence.

15 A. Brinkmann and M. H. Levitt, Symmetry principles in the nuclear magnetic resonance of spinning solids: heteronuclear recoupling by generalized Hartmann-Hahn sequences, *J. Chem. Phys.*, 2001, **115**, 357–384.
16 M. Edén, Advances in Symmetry-Based Pulse Sequences in Magic-Angle Spinning Solid-State NMR, *EMagRes*, 2007, 351–364.
17 M. H. Levitt, Symmetry in the design of NMR multiple-pulse sequences, *J. Chem. Phys.*, 2008, **128**, 052205.
18 N. C. Nielsen, L. A. Strassø and A. B. Nielsen, Dipolar recoupling, in *Solid State NMR*, 2012, pp. 1–45.
19 E. R. Andrew, A. Bradbury, R. G. Eades and V. T. Wynn, Nuclear cross-relaxation induced by specimen rotation, *Phys. Lett.*, 1963, **4**, 99–100.
20 E. R. Andrew, S. Clough, L. F. Farnell, T. D. Gledhill and I. Roberts, Resonant rotational broadening of nuclear magnetic resonance spectra, *Phys. Lett.*, 1966, **21**, 505–506.
21 D. P. Raleigh, G. S. Harbison, T. G. Neiss, J. E. Roberts and R. G. Griffin, Homonuclear Jcouplings and rotationally inducedsideband enhancements in NMR spectra of rotating solids, *Chem. Phys. Lett.*, 1987, **138**, 285–290.
22 D. P. Raleigh, M. H. Levitt and R. G. Griffin, Rotational resonance in solid state NMR, *Chem. Phys. Lett.*, 1988, **146**, 71–76.
23 D. P. Raleigh, F. Creuzet, S. K. Das Gupta, M. H. Levitt and R. G. Griffin, Measurement of internuclear distances in polycrystalline solids: rotationally enhanced transfer of nuclear spin magnetization, *J. Am. Chem. Soc.*, 1989, **111**, 4502–4503.
24 Z. Gan and D. M. Grant, Pseudo-spin rotational resonance and homonuclear dipolar NMR of rotating solids, *Mol. Phys.*, 1989, **67**, 1419–1430.
25 A. Kubo and C. A. McDowell, Spectral spin diffusion in polycrystalline solids under magicangle spinning, *J. Chem. Soc., Faraday Trans. 1*, 1988, **84**, 3713–3730.
26 M. H. Levitt, D. P. Raleigh, F. Creuzet and R. G. Griffin, Theory and simulations of homonuclear spin pair systems in rotating solids, *J. Chem. Phys.*, 1990, **92**, 6347–6364.
27 M. G. Colombo, B. H. Meier and R. R. Ernst, Rotor-driven spin diffusion in natural-abundance ^{13}C spin systems, *Chem. Phys. Lett.*, 1988, **146**, 189–196.
28 P. T. F. Williamson, A. Verhoeven, M. Ernst and B. H. Meier, Determination of internuclear distances in uniformly labeled molecules by rotational-resonance solid-state NMR, *J. Am. Chem. Soc.*, 2003, **125**, 2718–2722.
29 M. Helmle, Y. Lee, P. Verdegem, X. Feng, T. Karlsson, J. Lugtenburg, H. De Groot and M. Levitt, Anomalous rotational resonance spectra in magic-angle spinning NMR, *J. Magn. Reson.*, 1999, **140**, 379–403.
30 P. R. Costa, B. Sun and R. G. Griffin, Rotational resonance NMR: separation of dipolar coupling and zero quantum relaxation, *J. Magn. Reson.*, 2003, **164**, 92–103.
31 R. R. Ernst, G. Bodenhausen and A. Wokaun, *Principles of Nuclear Magnetic Resonance in One and Two Dimensions*, Oxford University Press, 1990.
32 R. Ramachandran, V. Ladizhansky, V. S. Bajaj and R. G. Griffin, ^{13}C–^{13}C Rotational ResonanceWidth Distance Measurements in Uniformly ^{13}C-Labeled Peptides, *J. Am. Chem. Soc.*, 2003, **125**, 15623–15629.
33 P. C. van der Wel, M. T. Eddy, R. Ramachandran and R. G. Griffin, Targeted ^{13}C–^{13}C Distance Measurements in a Microcrystalline Protein via J-Decoupled Rotational ResonanceWidth Measurements, *ChemPhysChem*, 2009, **10**, 1656–1663.
34 R. Janik, X. Peng and V. Ladizhansky, ^{13}C–^{13}C distance measurements in U-^{13}C, ^{15}N-labeled peptides using Rotational Resonance Width Experiment with a homogeneously broadened matching condition, *J. Magn. Reson.*, 2007, **188**, 129–140.
35 X. Peng, D. Libich, R. Janik, G. Harauz and V. Ladizhansky, Dipolar chemical shift correlation spectroscopy for homonuclear carbon distance measurements in proteins in the solid state: application to structure determination and refinement, *J. Am. Chem. Soc.*, 2008, **130**, 359–369.
36 R. Ramachandran, J. R. Lewandowski, P. C. van der Wel and R. G. Griffin, Multipolemultimode Floquet theory of rotational resonance width experiments: ^{13}C–^{13}C distance measurements in uniformly labeled solids, *J. Chem. Phys.*, 2006, **124**, 214107.
37 M. K. Pandey and R. Ramachandran, A theoretical perspective on the accuracy of rotational resonance (R^2)-based distance measurements in solid-state NMR, *Mol. Phys.*, 2010, **108**, 619–635.
38 M. K. Pandey and R. Ramachandran, Operator-based analytic theory of decoherence in NMR, *Mol. Phys.*, 2011, **109**, 1545–1565.
39 L. Sonnenberg, S. Luca and M. Baldus, Multiple-spin analysis of chemical-shift-selective (^{13}C, ^{13}C) transfer in uniformly labeled biomolecules, *J. Magn. Reson.*, 2004, **166**, 100–110.
40 R. Ramesh and M. S. Krishnan, Effective Hamiltonians in Floquet theory of magicangle spinning using van Vleck transformation, *J. Chem. Phys.*, 2001, **114**, 5967–5973.
41 U. SivaRanjan and R. Ramachandran, Unraveling multi-spin effects in rotational resonance nuclear magnetic resonance using effective reduced density matrix theory, *J. Chem. Phys.*, 2014, **140**, 054101.
42 R. Garg and R. Ramachandran, On the exactness of effective Floquet Hamiltonians employed in solid-state NMR spectroscopy, *J. Chem. Phys.*, 2017, **146**, 184201.
43 R. Garg and R. Ramachandran, Theory of coherent averaging in magnetic resonance using effective Hamiltonians, *J. Chem. Phys.*, 2020, **153**, 034106.
44 S. Ganguly, R. Garg and R. Ramachandran, On the equivalence between different averaging schemes in magnetic resonance, *J. Chem. Phys.*, 2020, **153**, 094103.
45 M. Mehring, *Principles of High-Resolution NMR in Solids*, Springer, Berlin, 1983.
46 M. Maricq and J. S. Waugh, NMR in rotating solids, *J. Chem. Phys.*, 1979, **70**, 3300–3316.
47 S. A. Smith, W. E. Palke and J. T. Gerig, The Hamiltonians of NMR. part I, *Concepts Magn. Reson.*, 1992, **4**, 107–144.
48 I. I. Rabi, Space quantization in a gyrating magnetic field, *Phys. Rev.*, 1937, **51**, 652–654.

Open Access Article. Published on 20 May 2025. Downloaded on 5/7/2026 11:37:47 PM.
This article is licensed under a Creative Commons Attribution-NonCommercial 3.0 Unported Licence.

49 W. Magnus, On the exponential solution of differential equations for a linear operator, *Commun. Pure Appl. Math.*, 1954, **7**, 649–673.
50 M. Veshtort and R. G. Griffin, SPINEVOLUTION: a powerful tool for the simulation of solid and liquid state NMR experiments, *J. Magn. Reson.*, 2006, **178**, 248–282.
51 P. Caravatti, G. Bodenhausen and R. R. Ernst, Selective pulse experiments in high-resolution solid state NMR, *J. Magn. Reson.*, 1983, **55**, 88–103.
52 M. Bansal and R. Ramachandran, Theory of finite pulse effects beyond perturbation limit: Challenges and Perspectives, *J. Magn. Res. Open*, 2022, **10–11**, 100042.
53 G. B. Arfken, H. J. Weber and F. E. Harris, *Mathematical Methods for Physicists*, Academic Press, Elsevier, 7th edn, 2013.
54 J. H. Shirley, Solution of the Schrödinger equation with a Hamiltonian periodic in time, *Phys. Rev.*, 1965, **138**, B979.
55 D. Suter and R. R. Ernst, Spin diffusion in resolved solid-state NMR spectra, *Phys. Rev. B: Condens. Matter Mater. Phys.*, 1985, **32**, 5608–5627.
56 K. Takegoshi, S. Nakamura and T. Terao, ^{13}C–^{1}H dipolar-assisted rotational resonance in magic-angle spinning NMR, *Chem. Phys. Lett.*, 2001, **344**, 631–637.
57 K. Takegoshi, S. Nakamura and T. Terao, ^{13}C–^{1}H dipolar-driven ^{13}C–^{13}C recoupling without ^{13}C RF irradiation in nuclear magnetic resonance of rotating solids, *J. Chem. Phys.*, 2003, **118**, 2325–2341.
58 C. R. Morcombe, V. Gaponenko, R. A. Byrd and K. W. Zilm, Diluting abundant spins by isotope edited radio frequency field assisted diffusion, *J. Am. Chem. Soc.*, 2004, **126**, 7196–7197.
59 M. Wilhelm, H. Feng, U. Tracht and H. W. Spiess, 2d CP/MAS ^{13}C isotropic chemical shift correlation established by ^{1}H spin diffusion, *J. Magn. Reson.*, 1998, **134**, 255–260.
60 A. Lange, S. Luca and M. Baldus, Structural constraints from proton-mediated rare-spin correlation spectroscopy in rotating solids, *J. Am. Chem. Soc.*, 2002, **124**, 9704–9705.
61 P. J. Carroll, P. L. Stewart and S. J. Opella, Structures of two model peptides: *N*-acetyl-D,L-valine and *N*-acetyl-L-valyl-L-leucine, *Acta Crystallogr., Sect. C: Cryst. Struct. Commun.*, 1990, **46**, 243–246.
62 A. Afrough, N. V. Christensen, R. W. M. Jensen, D. W. Juhl and T. Vosegaard, Magic angle spinning effects on longitudinal NMR relaxation: ^{15}N in L-histidine, *AIP Adv.*, 2023, **13**, 115123.

This journal is © the Owner Societies 2025